*Work jointly supported by the U.S. National Bureau of Standards, University Grants Commission and CSIR, India.

[1] W. Kohn, in *Solid States Phys.*, edited by F. Seitz and D. Turnbull (Academic, New York, 1958), Vol. 5, p. 257.
[2] R. W. Keyes, Phys. Rev. **122,** 1171 (1961).
[3] A. Griffin and P. Carruthers, Phys. Rev. **131,** 1976 (1963).
[4] P. C. Kwok, Phys. Rev. **149,** 666 (1966).
[5] H. Hasegawa, Phys. Rev. **118,** 1526 (1961).
[6] J. P. Dismukes, L. Ekstrom, E. F. Steigmeier, K. Kudman, and D. S. Beers, J. Appl. Phys. **35,** 2899 (1964).
[7] E. F. Steigmeier and B. Abeles, Phys. Rev. **136,** A1149 (1964).
[8] N. K. S. Gaur, C. M. Bhandari, and G. S. Verma, Phys. Rev. **144,** 628 (1965).
[9] J. F. Goff and N. Pearlman, Phys. Rev. **140,** A2151 (1965).
[10] N. K. S. Gaur and G. S. Verma, Phys. Rev. **159,** 610 (1967).
[11] P. G. Klemens, in *Solid State Physics*, edited by F. Seitz and D. Turnbull (Academic, New York, 1958), Vol. 7.
[12] P. Carruthers, Rev. Mod. Phys. **33,** 92 (1961).
[13] J. Callaway, Phys. Rev. **113,** 1046 (1959).

PHYSICAL REVIEW B VOLUME 2, NUMBER 12 15 DECEMBER 1970

Configuration Mixing of Subsidiary Minima: Corrections to the Ground-State Wave Function for Donors in Silicon*

T. G. CASTNER, JR.†
Department of Physics and Astronomy, University of Rochester, Rochester, New York 14627

(Received 18 February 1970)

The introduction of wave-function components from the region of the L_1, K_1, and U_1 points of the lowest conduction band into the ground-state wave function of the shallow donors As, P, and Sb is shown to improve substantially the agreement between the calculated Fermi contact constants for identified ENDOR shells and the experimental Fermi contact constants measured by Hale and Mieher. This wave-function admixture is the band-structure analogy to configuration mixing in atomic physics, and is calculated here employing first-order perturbation theory, the total impurity potential being the perturbing interaction. If one considers the low-energy L_1, K_1, and U_1 regions as subsidiary minima (strictly correct only for the L_1 region), this approach represents a logical extension of the Kohn-Luttinger formalism. This admixture of subsidiary minima is donor dependent (largest for As, intermediate for P, smallest for Sb) and is able to explain satisfactorily the numerous observed donor anomalies, even including the inverted-order cases. The calculated results indicate the positive identification of two new ENDOR shells, shell C as site (5, 5, 5) and shell F as site (2, 2, 0), and suggest the tentative identification of nine other ENDOR shells with lattice sites. Matching experimental Fermi contact constants and calculated values versus $k_0/k_{\max}$ for positively and tentatively identified ENDOR shells yields $k_0/k_{\max}=0.87\pm0.01$. A noninversion component of wave function has been introduced, resulting from the tetrahedral potential admixing $4f$-nf wave function (satisfying A_1 symmetry) into the solution of the single-valley Schrödinger equation. This addition makes only a slight improvement in the over-all agreement. The subsidiary-minima-admixture approach has also been attempted for the deep donor S^+, yielding an improved qualitative agreement between theory and experiment. The admixture of subsidiary minima has a number of other physical consequences: (1) The donor-nucleus hyperfine interaction can be reasonably accounted for, including the donor dependence, without employing the sharply peaked Whittaker function and a cutoff radius; (2) the "shear" deformation potential Ξ_u determined by ESR or optical experiments using the $1s$-A_1 donor ground state may not yield the true "shear" deformation potential of the Δ_1 minima; (3) the energy of the $1s$-A_1 state contains an important second-order correction from the subsidiary minima which can account for between 25% and 50% of the energy correction to the effective-mass value. It is shown the valley-valley coupling terms account for nearly all the energy correction of the $1s$-A_1 state, and that the single-valley correction is very small, contrary to previous work. Analysis of the location of the lattice sites positively and tentatively identified with ENDOR shells yields evidence that the three-dimensional appearance of the wave-function density of the $1s$-A_1 state significantly reflects the tetrahedral symmetry of the atoms surrounding the donor.

I. INTRODUCTION

The generally accepted treatment of the energy levels and wave functions of shallow donors and acceptors in semiconductors has been that developed by Kohn and Luttinger.[1] This elegant theory has been very successful when applied to the excited states of donors and acceptors; however, marked deviations have been observed[2] for the $1s$ states (particularly in silicon), most notably for the $1s$-A_1 ground state. These deviations have been attributed to central-cell corrections[3] and a number of attempts of several different types[4–9] have been made to calculate the corrected energy of the ground state. Efforts to correct the wave function have been made by Kohn and Luttinger[4] and also Muller[8] in an effort to explain the much larger wave-function density at the donor nucleus obtained from the hyperfine interaction with the donor nucleus.[10] Recently, a substantial amount of remarkable experimental data concerning the shallow donors As, P, and Sb in silicon has been reported by Hale and Mieher[11] (hereafter designated as HM I) using the ENDOR

technique. These data, consisting of an additional 15 shells (Fermi contact hyperfine constants and dipole-dipole constants composing the hyperfine tensors), in addition to the original five shells measured by Feher,[12] give a large amount of information on the wave function of the donor $1s$-A_1 ground state. These new data give much more information on the nature of the corrections required for the ground state than either the energy deviation or the magnitude of the wave-function density determined from the hyperfine interaction with the donor nucleus. It is these results that have provided the primary motivation for the corrections to the wave function of the ground state proposed in this paper.

In Feher's original ENDOR study[12] of As, P, and Sb donors in silicon, in which the hyperfine tensor components of five shells (at lattice sites occupied by Si^{29} nuclei) surrounding the donor were determined, a theory of the Fermi contact hyperfine interaction for the $1s$-A_1 ground state based on equal admixtures of wave function due to the six Δ_1 conduction-band minima was employed[13] to account for the data. The expression for the Fermi contact constant $a(\mathbf{r}_l)$ contained k_0, the wave number at the Δ_1 minimum, as a parameter. Feher was able to assign correctly three of the five observed ENDOR shells for the three donors and the analysis yielded an average value $k_0/k_{\max}=(0.85\pm0.03)$. Nevertheless, the fit of shells A [identified as (0, 0, 4)] and B [identified as (4, 4, 0)] required different k_0 values, the difference being greatest for As and smallest for Sb, the same order as for the deviation of the ionization energy from the effective-mass value. Feher's results did provide evidence for the strong interference involved in the wave-function density $|\psi(\mathbf{r}_l)|^2$ since the Fermi contact constant $a(\mathbf{r}_l)$ for shell E [identified as the nearest-neighbor shell (1, 1, 1) by the magnitude of the dipole-dipole constants] was approximately an order of magnitude smaller than those for shell A [identified as (0, 0, 4), the fourth nearest neighbor].

Hale and Mieher[14] (hereafter referred to as HM II) have used a similar theoretical analysis in an effort to explain their extensive experimental results. They have been able to show that the distribution of observed shells in the four different symmetry classes of shells is in good agreement with the calculated distribution, but they have been able to match only one new shell, namely, shell K as (0, 0, 8).[15] They have concluded that the present theory is sufficiently inaccurate to justify matching other shells. Thus, only four shells, A, B, E, and K, of the 20 or more observed shells have been positively identified. HM II concludes there are three major difficulties with the theory of the Fermi contact constant: (1) The shells cannot be matched with a single value of k_0; (2) the wave function should not, in general, have inversion symmetry; (3) the numerous observed donor anomalies [the order of the $a(\mathbf{r}_l)$ values not descending from As to Sb, as do the ionization energies] cannot be explained by the present wave function. In an effort to obtain more experimental information to assist in the matching of the observed shells with specific lattice sites, Hale and Castner[16] (hereafter designated as HC) have applied uniaxial stress along a cubic axis and observed shifts and splittings of most of the shells reported in HM I. The {110}-plane class of shells [shells for sites (n, n, m), $n\neq0$; most of the unidentified shells are in this class] all show different linear splittings with uniaxial stress, while the ⟨111⟩-axis-class shells showed quadratic shifts with stress. This uniaxial stress work has suggested the identification of one new shell, namely, shell Q, as (1, 1, 5). However, this study has also indicated that the calculated stress-induced shifts based on the present wave function cannot explain very much of the uniaxial stress data.[17]

It is the donor anomalies (observed in the Fermi contact constants, the dipole-dipole constants,[11,18] and also to some extent in the piezo-hyperfine constants determined by HC) which suggest that significant components of the $1s$-A_1 ground-state wave function are missing in the simple theory and that the amount of these missing additional components are donor dependent. In this paper we suggest that the admixed components are from the region of the higher subsidiary "minima" of the lowest conduction band at points L and K and also from the "saddle point" at $U(K')$ in the same band.[19] The admixture of wave function from these other points in the lowest conduction band is similar to the configuration mixing noted in atomic physics[20] and is calculated in this paper using first-order perturbation theory. The mixing interaction is the impurity potential, the central-cell portion being more important than the weak Coulombic potential. This approach represents a logical extension of the Kohn-Luttinger formalism for a many-valleyed conduction band and introduces only one new donor-dependent parameter per "minimum" admixed, assuming the shape of the band (the mass tensor) is known in the vicinity of the admixed point.

There has been some previous theoretical interest[21–23] in the question of subsidiary minima. (A formal treatment of the effect of secondary extrema in the band structure on impurity states has recently been given by Bassani, Iadonisi, and Preziosi.[24]) This interest centered on the question of the existence of bound states associated with subsidiary minima. Kaplan[22] and also Peterson[23] have concluded that bound states may exist, providing the impurity potential is slowly varying. However, this paper presents, to the best of our knowledge, the first evidence for the admixture of wave-function density from subsidiary minima into the ground-state wave function of shallow donors. The possible extension of this idea to deeper donors[25] such as S^+ is also considered in this paper. It has been the numerous band-structure calculations on silicon by the pseudopotential method,[26–30] the $\mathbf{k}\cdot\mathbf{p}$

method,[31] and the Fourier series expansion approach[32] which have given an indication of the location of these subsidiary "minima" and their approximate energy above the Δ_1 absolute minima. Refinement of the calculations presented in this paper may permit the direct determination, using the ENDOR data, of the energy differences between the absolute minima and the subsidiary "minima" within the lowest conduction band.

In Sec. II the technique for adding wave-function components from subsidiary minima is developed. Section III explores the various physical consequences of the admixture of subsidiary minima into the donor ground-state wave function, including the effect on the determination of the "spin-resonance value" of the shear deformation potential constant.[33] Section IV presents the results of detailed calculations of the Fermi contact constants for approximately 25 shells for the As, P, and Sb donors in silicon, and suggests the identification of several new ENDOR shells with specific lattice sites. A brief discussion of the application of the method to the ENDOR results for the S^+ donor is given in Sec. V. Section VI discusses some additional situations where subsidiary minima might be considered and presents the major conclusions of this study.

II. DONOR WAVE FUNCTION—EXTENSION TO INCLUDE SUBSIDIARY MINIMA

A. General Considerations

The wave function for a bound state, ψ_b, can always be written as a linear combination of Bloch functions, namely,

$$\psi_b(\mathbf{r})=\sum_n \sum_{\mathbf{k}\text{ over BZ}} a_n(\mathbf{k})\psi_{n\mathbf{k}}, \tag{1}$$

where the Bloch function $\psi_{n\mathbf{k}}=u_{n\mathbf{k}}(\mathbf{r})\exp(i\mathbf{k}\cdot\mathbf{r})$ is for the nth band and $\mathbf{k}$ is the wave number; BZ stands for Brillouin zone. This bound-state wave function is a solution of the Schrödinger equation containing a Hamiltonian $H=H_0+U(\mathbf{r})$, where $U(\mathbf{r})$ is the impurity potential and H_0 includes $V(\mathbf{r})$, the periodic crystal potential. For the shallow donors the bound states have energies slightly less than the conduction-band edge (or edges, as in the multivalley semiconductors Si and Ge), and the wave-function component associated with the energy minima located at $\mathbf{k}_j$ in the band $n=0$ is given by

$$\psi_{bj}(\mathbf{r})=\sum_{\mathbf{k}} a_0(\mathbf{k}-\mathbf{k}_j)u_{0\mathbf{k}}(\mathbf{r})\exp(i\mathbf{k}\cdot\mathbf{r}). \tag{2}$$

In (2) the wave function has been limited to a single band, a very good approximation for donors in silicon as justified by Kohn.[34] Using the procedure of Kohn and Luttinger, this wave function is converted to a function of real space by the introduction of the envelope function $F_j(\mathbf{r})$, associated with this jth minimum, defined as

$$F_j(\mathbf{r})=\sum_{\text{all }\mathbf{k}} a_0(\mathbf{k}-\mathbf{k}_j)\exp[i(\mathbf{k}-\mathbf{k}_j)\cdot\mathbf{r}]. \tag{3}$$

The function $F_j(\mathbf{r})$ is just the Fourier transform of $a_0(\mathbf{k}-\mathbf{k}_j)$. A second approximation has been introduced by extending the $\mathbf{k}$ summation over all $\mathbf{k}$ space, which is justified by the very sharp peaking of $a_0(\mathbf{k}-\mathbf{k}_j)$ about k_j. The transformation of the Schrödinger equation $H\psi_{bj}=E\psi_{bj}$ by Fourier transforms leads to the single-valley effective-mass Schrödinger equation for $F_j(\mathbf{r})$, namely,

$$[E_j(i\nabla)+U(\mathbf{r})]F_j(\mathbf{r})=EF_j(\mathbf{r}), \tag{4}$$

where the impurity potential $U(\mathbf{r})$ is given by

$$U(\mathbf{r})=-e^2/\epsilon_0 r+\delta U(\mathbf{r}). \tag{5}$$

ϵ_0 is the static dielectric constant, while $\delta U(\mathbf{r})$ is the extra "central-cell" potential[35] (attractive for As, P, Sb, and Bi). Neglecting δU and assuming a quadratic energy dependence for $E_j(i\nabla)$ for a z-axis valley, namely,

$$E_z(i\nabla)=-\frac{\hbar^2}{2m_t}\frac{\partial^2}{\partial z^2}-\frac{\hbar^2}{2m_t}\left(\frac{\partial^2}{\partial x^2}+\frac{\partial^2}{\partial y^2}\right), \tag{6}$$

Kohn and Luttinger[1] employed a variational wave function and found the effective-mass eigenvalue $E_0=-29$ meV. For silicon with its six Δ_1 conduction-band minima the bound-state wave functions have the form

$$\psi_b=\sum_{j=1}^{6}\alpha_j F_j(\mathbf{r})u_{\mathbf{k}_j}(\mathbf{r})\exp(i\mathbf{k}_j\cdot\mathbf{r}), \tag{7}$$

where $u_{\mathbf{k}_j}(\mathbf{r})\exp(\mathbf{k}_j\cdot\mathbf{r})$ is the Bloch function associated with the jth minimum. The α_j are numerical coefficients determined by the tetrahedral symmetry. For the $1s$-A_1 ground state (totally symmetric in the sum over valleys) the $\alpha_j=\sqrt{\frac{1}{6}}$. We also note that the overlap between the different Δ_1 minima has been neglected in constructing $\psi_b(\mathbf{r})$. This is justified by the rapid decrease of $a_0(\mathbf{k}-\mathbf{k}_j)$ away from the minima.

As noted, the energy of the $1s$-A_1 donor states deviates substantially from $E_0=-29$ meV due to central-cell corrections. In fact, the corrections to the energy of the $1s$ donor states present a very complex problem.[36] Several attempts to correct the $F_j(\mathbf{r})$ using the single-valley Schrödinger equation (the coupling between valleys was not considered) in Eq. (4) have been made.[4,8] These efforts resulted in a corrected $F_j(\mathbf{r})$ that was substantially more peaked for small r than the wave function $(1/\pi a^{*3})^{1/2}\exp[-(r/a^*)]$ (assumed isotropic here for simplicity; $a^*\sim 20$ Å) associated with E_0.

A compact formulation of the wave function for the unpaired electron of the shallow donors has been achieved. The following assumptions were made: (1) bands other than the lowest conduction band can be neglected; (2) sums of $\mathbf{k}$ over the first BZ can be extended over all $\mathbf{k}$ space; (3) the $a_0(\mathbf{k}-\mathbf{k}_j)$ are only

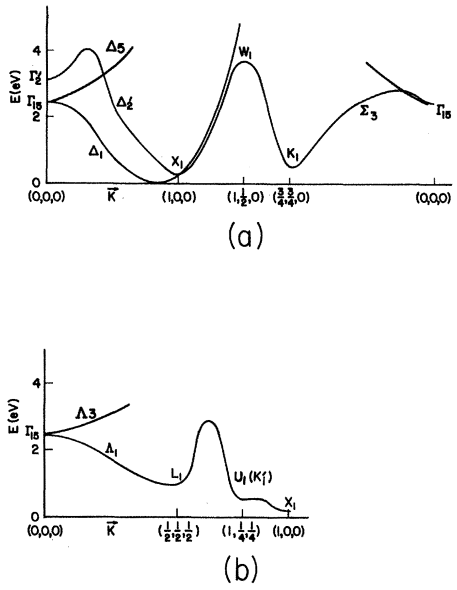

FIG. 1. Band structure in the vicinity of the lowest conduction band of silicon according to Refs. 26–32. While quantitative differences exist between the various calculations, the qualitative features are in reasonable agreement. (a) $E(\mathbf{k})$ along Δ, Z, WK, and Σ; (b) $E(\mathbf{k})$ along Λ, LU, and $UX(\Sigma')$.

large in a small region of k space surrounding the absolute minima of the lowest conduction band. This third assumption is a direct consequence of assuming $E_j(\mathbf{k}-\mathbf{k}_j)$ is quadratic in $(\mathbf{k}-\mathbf{k}_j)$ and the weak Coulombic potential. Consequently, for a multivalley semiconductor with conduction-band minima far apart, $a_0(\mathbf{k}-\mathbf{k}_j)$ is negligible midway between two minima. It was not explicitly stated, but it was implied that the contribution from higher-energy minima of the lowest conduction band could be neglected. It is this aspect of the third assumption that is thought to need correction. Inspection of the calculated band structures for silicon[26–32] indicates a large number of subsidiary "minima" and "saddle points" one eV or less above the Δ_1 minima.

B. Lowest Conduction Band of Silicon

In Fig. 1 the important features of the lower-energy portion of the silicon conduction band are shown. The absolute minima occur along the cubic axes with $(k_0/k_{\max})=0.86\pm0.02$. The band-structure calculations[26–32] indicate a minimum at L_1[37] and suggest a low-energy region of states in the vicinity of K_1 which will be considered as a "minimum"[38] in this work. Using the relationship $E_{\mathbf{k}+\mathbf{G}n}=E_{\mathbf{k}}$, where $\mathbf{G}_n$ is a reciprocal-lattice vector, one readily shows that the point U_1 (also designated[39] as K_1') has the same energy as K_1. (Also see Fig. 2; one K point is equivalent to two U points.) The band-structure calculations indicate that the energy must increase rapidly from U_1 to W_1 and it is also most likely that the energy increases from U_1 toward Γ_{15}. Kane's calculation[30] shows the energy to decrease monotonically from U_1 to X_1, implying that U_1 is a "saddle point" of the second type.[40] The band calculations indicate the point W_1 is a "maximum" and also show a maximum along K_1L_1 [also along U_1L_1 since $E(U_1L_1)=E(K_1L_1)$ employing $E_{\mathbf{k}+\mathbf{G}111}=E_{\mathbf{k}}$] on the hexagonal face. These 24 inequivalent points are either maxima, type-one, or type-two saddle points, depending on the energy variation from these points toward Γ_{15} and perpendicular to K_1L_1. The second possibility seems likely. This accounts for all the known "critical points" on the exterior of the BZ except for the X_1 points.[41]

In the interior there are 12 maxima along $\Gamma_{15}\Sigma_3$ and one at the origin. Application of Morse's rules[42] (taking into account degeneracy[43]) indicates there should be a large number of critical points, mostly saddle points, in the interior of the BZ.[44] In making corrections to the donor ground-state wave function, only the L_1, K_1, and U_1 points and their environs will be considered. It is unlikely that the higher-energy maxima or type-one saddle points make a significant contribution to the donor wave function; however, any low-energy type-two saddle points (or minima?) might make a noticeable contribution to the wave function. Not enough is known about interior critical points to consider them in the present work. Nevertheless, the possible importance of low-energy critical points in the interior on the donor ground-state wave function makes further consideration of the band structure in the interior worthwhile.

Table I shows the energy of some of these points, based on the effective-mass expression, relative to the Δ_1 minima given by

$$E_{\text{eff mass}}=\frac{\hbar^2 k_{\max}^2}{2m}\times\left\{\frac{m}{m_t}\frac{(k_z-k_0)^2}{k_{\max}^2}+\frac{m}{m_t}\frac{(k_x^2+k_y^2)}{k_{\max}^2}\right\}, \quad (8)$$

where $k_{\max}=2\pi/a$ (the lattice constant $a=5.43$ Å).

TABLE I. Energy of high symmetry points of the lowest conduction band in silicon (measured with respect to the Δ_1 minima).

Point in BZ	$E_{\text{eff mass}}$ eV	$E_{\text{band calc}}$[a] eV	$a_0(\mathbf{k}-k_0\mathbf{i}_z)/a_0(0)$
$X_1-(0,0,1)k_{\max}$	0.12	0.15–0.3	1.7×10^{-2}
$W_1-(0,\frac{1}{2},1)k_{\max}$	6.97	2.8–4.1	2.16×10^{-5}
$U_1(K_1')$ $-(\frac{1}{4},\frac{1}{4},1)k_{\max}$	3.55	0.4–0.8	7.54×10^{-5}
$K_1-(0,\frac{3}{4},\frac{3}{4})k_{\max}$	15.2	0.4–0.8	4.6×10^{-6}
$L_1-(\frac{1}{2},\frac{1}{2},\frac{1}{2})k_{\max}$	14.3	0.5–1.3	5.05×10^{-6}
$\Gamma_{15}-(0,0,0)k_{\max}$	4.2	2.1–2.5	2.3×10^{-5}

[a] Based on calculations in Refs. 26–32.

The results of the band calculations are also shown for these points. Also shown in Table I is the relative amplitude $a_0(\mathbf{k}-k_0\mathbf{i}_z)/a_0(0)$ of the Bloch function admixture based on the effective-mass envelope function $F_z(r)$ used by Kohn and Luttinger[1] in their variational calculation. This quantity is given by

$$a_0(\mathbf{k}-k_0\mathbf{i}_z)/a_0(0)=1/[1+(k_z-k_0)^2b^2+(k_x^2+k_y^2)a^2]^2, \tag{9}$$

where $k_{\max}b=16.4$ and $k_{\max}a=28.8$.

Table I suggests that the effective-mass energy is a reasonable approximation along Δ_1, both toward X_1 and Γ_{15}. It gives an overestimate of the energy at W_1, but the dependence along X_1W_1 is satisfactory. However, the effective-mass energy at U_1 is a factor of $4\frac{1}{2}$ to 9 times larger than the calculations; at L_1 it is 10 to 30 times larger; at K_1 it is 20 to 40 times larger. At the points L_1, K_1, and U_1, the actual band energy is much less than that assumed by effective-mass theory. Inspection of the factor $a_0(\mathbf{k}-k_0\mathbf{i}_z)/a_0(0)$ at these three points shows it is very small ($<10^{-4}$ at U_1, $<10^{-5}$ at K_1 and L_1). Even with increases of 10^2 or more, the values of $a_0(\mathbf{k}-k_0\mathbf{i}_z)/a_0(0)$ would seem too small to have much effect on the wave function after the sum over $\mathbf{k}$ in Eq. (1) is performed. This conclusion is misleading and not to the point. In fact, there is a large density of states associated with the region surrounding these three symmetry points. Considerably more of the BZ is in the vicinity of these three points than in the vicinity of the six Δ_1 minima. It remains to be shown that these regions are strongly enough coupled to the Δ_1 minima to make a measurable contribution to the ground-state donor wave function.

C. Configuration Mixing of Subsidiary Valleys

The impurity potential $U(\mathbf{r})$ in Eq. (4) will couple the Kohn-Luttinger wave function ψ_{KL} based on the six Δ_1 minima given in Eq. (7) with the wave function associated with the mth subsidiary valley or minimum located at $\mathbf{k}_m$. The valley wave function for the mth valley will have the form $\psi_m=F_m(\mathbf{r})u_{\mathbf{k}_m}(\mathbf{r})\exp(i\mathbf{k}_m\cdot\mathbf{r})$, where $F_m(\mathbf{r})$ [defined in Eq. (3)] is the solution of the one-valley Schrödinger equation employing $E(\mathbf{k}-\mathbf{k}_m)$ to find the kinetic-energy operator. The corrected ground-state wave function employing first-order perturbation theory will be

$$\psi_{1s-A_1)t}=(N_{A_1})^{-1/2}\times\left[\psi_{KL-1s-A_1}+\sum_m\frac{\langle\psi_m\mid U(\mathbf{r})\mid\psi_{KL-1s-A_1}\rangle\psi_m}{(E_{1s-A_1)\Delta_1}-E_{1s-\mathbf{k}_m})}\right], \tag{10}$$

where the sum is over all higher-energy subsidiary valleys under consideration and N_{A_1} is a normalization constant. The difference in energy of the donor $1s$-A_1 state of the Δ_1 minima and the mth valley (measured with respect to the respective edges) is small in comparison with the energy difference between the respective "critical" points, so that the energy denominator is well approximated by $E_{\Delta_1}-E_{\mathbf{k}_m}$. For a particular symmetry set of subsidiary valleys, the totally symmetric summation over the six Δ_1 valleys in $\psi_{KL-1s-A_1}$ requires that the matrix elements $\langle\psi_m\mid U(\mathbf{r})\mid\psi_{KL-1s-A_1}\rangle$ have the same magnitude,[45] which suggests the use of wave functions $\mid A_1\rangle_M$ which are totally symmetric summations over the respective ψ_m, namely (dropping the $1s$),

$$\mid A_1\rangle_M=(1/N_M)^{1/2}\sum_m F_m(\mathbf{r})u_{\mathbf{k}_m}(\mathbf{r})\exp(i\mathbf{k}_m\cdot\mathbf{r}), \tag{11}$$

where $N_M=4$, 12, and 24 for the L_1, K_1, and U_1 valleys, respectively. The corrections from the L_1, K_1, and U_1 regions make the total corrected ground-state A_1 wave function become

$$\mid A_1\rangle_t=(1/N_{A_1})^{1/2}\times[\mid A_1\rangle_{\Delta_1}+\alpha_L\mid A_1\rangle_{L_1}+\alpha_K\mid A_1\rangle_{K_1}+\alpha_U\mid A_1\rangle_{U_1}], \tag{12}$$

where $\mid A_1\rangle_{\Delta_1}=\psi_{KL-1s-A_1}$ and the admixture coefficients α_M [not to be confused with the α_j in Eq. (7)] are given by

$$\alpha_M\simeq\langle A_{1-M}\mid U(\mathbf{r})\mid A_{1-\Delta_1}\rangle/(E_{\Delta_1}-E_{\mathbf{k}_m}). \tag{13}$$

These α_M can be shown to be real positive constants.[45] Neglecting overlap between all valleys (as in $\psi_{KL-1s-A_1}$), the normalization constant takes the form $N_{A_1}=1+\alpha_L^2+\alpha_K^2+\alpha_U^2$ if the individual $\mid A_1\rangle_M$ are normalized.

For the L_1 valleys (true minima), the situation is just as for donor states in Ge, namely, these valleys are fourfold degenerate yielding a totally symmetric A_1 state and triplet T_2 states. For the 12 K_1 valleys (low-energy pockets, but not minima)[44] the 12-fold symmetry is split in T_d symmetry into $A_1+E+T_1+2T_2$. The U_1 "valleys" (which resemble saddle points) split in a similar manner to the K_1 valleys. Since the K_1 and U_1 valleys are not minima, the wave functions $\mid A_1\rangle_{K_1}$ and $\mid A_1\rangle_{U_1}$ are only approximate corrections[44] for these

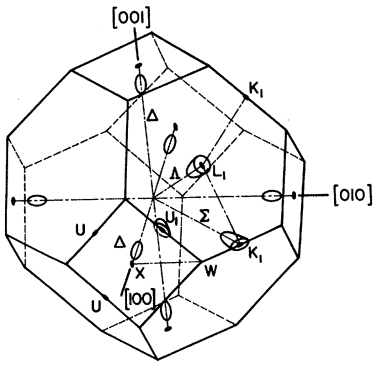

FIG. 2. Brillouin zone of silicon showing the six Δ_1 minima along the cubic axes and the position of the subsidiary "minima" considered in this paper. L_1 is a true minimum characterized by two mass components. K_1 is not a true minimum, but is a low-energy valley. The U_1 region approximates a saddle-point region.

portions of the BZ. We have treated the K_1 and U_1 regions separately rather than considering one K_1 and two U_1 valleys (two U points are related to each K point by reciprocal-lattice vectors) to constitute a single "valley." This is justified and preferable because (1) the $F_m(\mathbf{r})$ for these valleys involve $\mathbf{k}$ summations over only the first BZ (higher bands neglected), and the $F_m(\mathbf{r})$ for the K_1 and U_1 regions differ because $E(\mathbf{k}-\mathbf{k}_m)$ does not vary in the same way around these points; (2) the coupling of the K_1 and U_1 valleys with the Δ_1 valleys is different; (3) $|A_1\rangle_{K_1}$ and $|A_1\rangle_{U_1}$ do not give equivalent results for the odd-integer and the even-integer lattice sites (see Table III, below).

If we consider only the s part of $u_{\mathbf{k}_m}(\mathbf{r})$ for all the valleys (the only part which contributes to the Fermi contact constant, which is always mixed in phase with $|A_1\rangle_{\Delta_1}$), then $u_{\mathbf{k}_m}(\mathbf{r})$ will be the same for all valleys of the same symmetry set and can be factored out of $|A_1\rangle_M$. In this case, $|A_1\rangle_{L_1}$, $|A_1\rangle_{K_1}$, and $|A_1\rangle_{U_1}$ have the form

$$|A_1\rangle_{L_1}=[2u_{L_1}(\mathbf{r})/(4)^{1/2}][F_{xyz}\cos(\pi/a)(x+y+z)+F_{xy\bar{z}}\cos(\pi/a)(x+y-z)+F_{x\bar{y}z}\cos(\pi/a)(x-y+z)+F_{\bar{x}yz}\cos(\pi/a)(-x+y+z)], \quad (14a)$$

$$|A_1\rangle_{K_1}=[2u_{K_1}(\mathbf{r})/(12)^{1/2}][F_{xy}\cos(3\pi/2a)(x+y)+F_{x\bar{y}}\cos(3\pi/2a)(x-y)+F_{yz}\cos(3\pi/2a)(y+z)+F_{y\bar{z}}\cos(3\pi/2a)(y-z)+F_{zx}\cos(3\pi/2a)(z+x)+F_{z\bar{x}}\cos(3\pi/2a)(z-x)], \quad (14b)$$

$$|A_1\rangle_{U_1}=[2u_{U_1}(\mathbf{r})/(24)^{1/2}][F_{Xyz}\cos(\pi/2a)(4x+y+z)+F_{Xy\bar{z}}\cos(\pi/a)(4x+y-z)+F_{X\bar{y}z}\cos(\pi/a)(4x-y+z)+F_{X\bar{y}\bar{z}}\cos(\pi/2a)(4x-y-z)+8 \text{ similar terms for } F_{xYz}, \text{ etc., and } F_{xyZ}, \text{ etc.}]. \quad (14c)$$

Similar corrections to the wave functions for the $1s$-E and $1s$-T_2 states will have the form

$$|E\rangle=(1/N_E)^{1/2}[|E\rangle_{\Delta_1}+\epsilon_K|E\rangle_{K_1}+\epsilon_U|E\rangle_{U_1}] \quad (15a)$$

and

$$|T_2\rangle=(1/N_{T_2})^{1/2}\times[|T_2\rangle_{\Delta_1}+\tau_L|T_2\rangle_{L_1}+\tau_K|T_2\rangle_{K_1}+\tau_U|T_2\rangle_{U_1}]. \quad (15b)$$

The ϵ's and τ's and the normalization coefficients are defined in the same manner as the α's and N_{A_1}. In Eq. (15a) there is no contribution from the L_1 minima because in T_d symmetry combinations of the L_1 valley functions yield only the A_1 and T_2 representations.

All of the α's, ϵ's, and τ's can be related to the individual matrix elements $\langle\psi_j|U(\mathbf{r})|\psi_i\rangle$ of the impurity potential between the valley wave functions for the ith and jth valleys. The procedure for doing this is given in Appendix A. The results suggest that the α's are much larger than the ϵ's and τ's because it is only the totally symmetric A_1 state where all the individual matrix elements $\langle\psi_j|U(\mathbf{r})|\psi_i\rangle$ add together. For the E and T_2 states there is substantial cancellation between the individual $\langle\psi_j|U(\mathbf{r})|\psi_i\rangle$. Because of the detailed ENDOR and ESR data for the $1s$-A_1 state we shall only be concerned with corrections to the A_1 wave function. Even though the individual $\langle\psi_j|U(\mathbf{r})|\psi_i\rangle$ may only be a few millivolts the totally symmetric sum over a large number of valleys can yield α's of the order $\frac{1}{10}$.

The neglect of overlap between different symmetry valleys is analogous to the neglect of overlap between the six Δ_1 minima [setting the α_j in Eq. (7) equal to $(\frac{1}{6})^{1/2}$]. Here the minima are closer in $\mathbf{k}$ space and the approximation is less valid, particularly for the overlap between the Δ_1 and adjacent U_1 valleys. An estimate of these overlap integrals is made in Appendix B. The neglect of the overlap integrals between the different valleys can be viewed as a "tight-binding" approximation applied to $\mathbf{k}$ space. The shallower the donor state, the larger the radius of the state, the smaller the amount of $\mathbf{k}$ space required to adequately describe the valley wave function, and thus the smaller the overlap between different valleys.

D. Fermi Contact Hyperfine Interaction

The Fermi contact hyperfine interaction[46] for a nucleus located at the site $\mathbf{r}_l$ with respect to the donor at $\mathbf{r}=0$ is given by

$$a(\mathbf{r}_l)=(8\pi/3)g\,g_n\mu_B\mu_{B_n}|\psi(\mathbf{r}_l)|^2. \quad (16)$$

For $\psi(\mathbf{r}_l)$ we substitute $|A_1\rangle_l$ from Eq. (12), thus obtaining

$$a(\mathbf{r}_l)=(8\pi/3N_{A_1})g\,g_n\mu_B\mu_{B_n}[|A_1(\mathbf{r}_l)\rangle_{\Delta_1}+\alpha_L|A_1(\mathbf{r}_l)\rangle_{L_1}+\alpha_K|A_1(\mathbf{r}_l)\rangle_{K_1}+\alpha_U|A_1(\mathbf{r}_l)\rangle_{U_1}]^2. \quad (17)$$

Employing Eqs. (14a)–(14c) we factor out of Eq. (17) the radial part of the Δ_1 minimum envelope function, $2u_\Delta(\mathbf{r}_l)/(6)^{1/2}$, and a quantity $I_\Delta(\mathbf{r}_l)$ which is yet to be defined. The resulting form for $a(\mathbf{r}_l)$ is

$$a(\mathbf{r}_l)=\frac{A_0}{N_{A_1}}\left(\frac{F_\Delta(\mathbf{r}_l)}{F_{a^*}(0)}\right)^2(\tfrac{1}{3}I_\Delta)^2\times\left[1+\beta_L\frac{I_L(\mathbf{r}_l)}{I_\Delta(\mathbf{r}_l)}+\beta_K\frac{I_K(\mathbf{r}_l)}{I_\Delta(\mathbf{r}_l)}+\beta_U\frac{I_U(\mathbf{r})}{I_\Delta(\mathbf{r}_l)}\right]^2, \quad (18)$$

where A_0 is a donor-independent effective-mass Fermi contact constant of a Si^{29} nucleus located at the origin due only to $|A_1\rangle_{\Delta_1}$, namely,

$$A_0=6\times(8\pi/3)g\,g_n\mu_B\mu_{B_n}\eta|F_{a^*}(0)|^2. \quad (19)$$

$\eta=|u_\Delta(\mathbf{r}_l)|^2/\langle|u_\Delta(r)|^2\rangle_{\text{av}}$ is a dimensionless factor[47] representing the concentration of periodic wave function at a silicon nucleus. $F_{a^*}(0)=(1/\pi a_\Delta{}^{*3})^{1/2}$, where $a_\Delta{}^*$ is the isotropic Bohr radius of $F_\Delta(r)$ neglecting all

corrections. The β_M are a new set of constants given by

$$\beta_M=\alpha_M(6/N_M)^{1/2}[u_M(\mathbf{r}_l)/u_\Delta(\mathbf{r}_l)], \quad M=L,\ K,\text{ and } U. \tag{20}$$

The $I_M(\mathbf{r}_l)$ factors in Eq. (18) are *valley interference factors* associated with the respective symmetry valleys and vary greatly with the position of the lattice site. They are defined by

$$I_M(\mathbf{r}_l)\equiv(N_M)^{1/2}[|\,A_1(\mathbf{r}_l)\rangle_M/2u_M(\mathbf{r}_l)F_\Delta(\mathbf{r}_l)] \tag{21}$$

and are simply sums of cosines times anisotropic envelope functions. These valley interference factors provide a compact means of determining the amount of wave function from a given symmetry set of valleys at a particular lattice site. They can be considered known quantities if the band structure is known, so that k_0 and the envelope functions for the different valleys can be determined.

The hyperfine interaction $a(\mathbf{r}_l)$ in Eq. (18) consists of the uncorrected part associated with just the six Δ_1 minima times a correction factor $1/N_{A_1}$ multiplied by the quantity in the square brackets. In this correction factor the $I_M(\mathbf{r}_l)$ factors depend almost entirely on the structure of the lowest conduction band in silicon while the β_M's depend on the potential $U(\mathbf{r})$ and the ratios $u_M(\mathbf{r}_l)/u_\Delta(\mathbf{r}_l)$. Only three potential-dependent constants are required to specify the amount of the wave-function admixture from these three subsidiary valley regions.

E. Dipole-Dipole Interactions

The dipole-dipole interaction hyperfine constants reported in HM I also contain a wealth of information about the donor ground-state wave function. However, there are more unknown parameters involved in these quantities and the inclusion of s, p, and d functions in the $u_{\mathbf{k}j}(\mathbf{r})$ makes for a large number of terms in the different integrations. A detailed consideration of the corrections to the dipole-dipole constants due to the other subsidiary minima will be considered in another paper. However, we include expressions for the dipole-dipole constants considering just the six Δ_1 minima in this paper because (1) they are useful in the identification of certain shells, and (2) they have been derived by an alternative method to the equivalent orbital technique employed by Hale and Mieher,[18] and in the case of the B_{zz} component includes a term not reported by Hale and Mieher.

The dipole-dipole constants are given by

$$B_{zz}=b_0\int[(x^2+y^2-2z^2)/r^5]\,|\,\psi_b\,|^2\,d\tau, \tag{22a}$$

$$B_{xy}=-3b_0\int(xy/r^5)\,|\,\psi_b\,|^2\,d\tau, \tag{22b}$$

$$B_{xz}=-3b_0\int(xz/r^5)\,|\,\psi_b\,|^2\,d\tau, \tag{22c}$$

where $b_0=g\,g_n\mu_B\mu_{Bn}$ and ψ_b is as in Eq. (7). The envelope functions $F_j(\mathbf{r})$ are very slowly varying functions compared with both the $u_{\mathbf{k}_j}(\mathbf{r})$ and the phase factors $\exp(i\mathbf{k}_j\cdot\mathbf{r})$. It is the rapid variation of both $u_{\mathbf{k}_j}(\mathbf{r})$ and the phase factors which accounts for most of the magnitude of the dipole-dipole constants.[48] The $F_j(\mathbf{r})$ are considered constant and equal to the value at the nucleus, $F_j(\mathbf{r}_l)$, while the $u_{\mathbf{k}_j}(\mathbf{r}_l+\mathbf{r})$ and the phase factors $\exp[i\mathbf{k}_j\cdot(\mathbf{r}_l+\mathbf{r})]$ are expanded about the lattice site at $\mathbf{r}_l$ in terms of a relative coordinate $\mathbf{r}$. Thus for the x-axis valley, $u_{\mathbf{k}_{0x}}(\mathbf{r}_l+\mathbf{r})$ has the form $s(\mathbf{r}_l+\mathbf{r})+p_x(\mathbf{r})+d_{yz}(\mathbf{r})+\cdots$,[49] while $\cos k_0(x_l+x)$ and $\sin k_0(x_l+x)$ are expanded exactly. The resulting $|\,\psi_b\,|^2$ contains a large number of terms of both the intravalley and intervalley type. Nevertheless, it can be shown that these dipole-dipole expressions can be reduced to the following:

$$B_{zz}(\mathbf{r}_l)=[F_x^2(\mathbf{r}_l)\cos^2k_0x_l+F_y^2(\mathbf{r}_l)\cos^2k_0y_l-2F_z^2(\mathbf{r}_l)\cos^2k_0z_l]J_1$$
$$+[2F_x(\mathbf{r}_l)F_y(\mathbf{r}_l)\cos k_0x_l\cos k_0y_l-F_x(\mathbf{r}_l)F_z(\mathbf{r}_l)\cos k_0x_l\cos k_0z_l-F_y(\mathbf{r}_l)F_z(\mathbf{r}_l)\cos k_0y_l\cos k_0z_l]J_2, \tag{23a}$$

$$B_{xy}(\mathbf{r}_l)=[F_x(\mathbf{r}_l)F_y(\mathbf{r}_l)\sin k_0x_l\sin k_0y_l]J_3$$
$$\pm\{F_z(\mathbf{r}_l)\sin k_0z_l[(F_x(\mathbf{r}_l)\cos k_0x_l+F_y(\mathbf{r}_l)\cos k_0y_l)J_4+(F_z(\mathbf{r}_l)\cos k_0z_l)J_4']\}, \tag{23b}$$

and

$$B_{xz}(\mathbf{r}_l)=B_{xz}(x_l,y_l,z_l)=B_{xy}(x_l,z_l,y_l). \tag{23c}$$

The integrals J_1, J_2, and J_3 contain the dipole-dipole operators and terms containing components of $u_{\mathbf{k}_j}(\mathbf{r})$ like $s\times s$, $p\times s$, and $p\times p$ times the corresponding sines and cosines. J_4 and J_4' arise only from $s\times d$ terms and the nearly identical form of the integrals indicates $J_4\simeq J_4'$. As noted by Hale and Mieher,[18] the magnitudes of these integrals are not readily obtained and might best be determined by fitting these expressions to identified shells like A and B. However, if the wave-function admixture from the subsidiary minima makes a significant correction to the dipole-dipole constants of these particular shells, incorrect values of the J's will be determined. We note that expressions (23b) and (23c) are identical to those obtained by the equivalent orbital technique, but that the second term[50] in (23a) resulting from cross terms between adjacent minima is apparently not found by the equivalent orbital technique. A close examination of the integrals J_1 and J_2 indicates they should be of the same order of magnitude. As discussed in Sec. IV, this extra term has a small effect for most shells, but for several specific shells can make the major contribution to B_{zz}.

Expressions (23a)–(23c) indicate that the dipole-dipole constants should all be proportional to $|\,F_\Delta(\mathbf{r}_l)\,|^2$

TABLE II. Wave-function density at donor nucleus.

Donor	Eff mass	$\lvert\psi(0)\rvert^2_{\text{calc}}\times10^{-24}$ cm^{-3} b^*	b^*-SM	b^*-SM_{corr}	$\lvert\psi(0)\rvert^2_{\text{expt}}\times10^{-24}$ cm^{-3}
As (1)	0.0546	0.137	0.495	1.24	1.73[a]
(2)	0.0531	0.133	0.630	1.58	
P (1)	0.0546	0.107	0.320		0.43[a]
(2)	0.0531	0.104	0.403		
Sb (1)	0.0546	0.0968	0.224	0.56	1.18[a]
(2)	0.0531	0.0940	0.340	0.85	

[a] G. Feher, Phys. Rev. 114, 1219 (1959).

and would be expected to exhibit donor anomalies consistent with the observed ground-state energy anomalies of As, P, and Sb. Furthermore, the donor anomalies should be smaller for the more distant shells. The data in HM I indicate that the dipole-dipole constants of many shells, but not all, are in agreement with these predictions, even in cases where the Fermi contact constants exhibit marked donor anomalies [see, for example, shells H, O, and X]. For shell A, B_{zz} has a donor anomaly similar to $a(\mathbf{r}_l)$, while B_{xy} does not have any unusual donor anomaly. For shell I, $a(\mathbf{r}_l)$, B_{zz}, and B_{xy} are normal while the B_{xz} constants are inverted (As<P<Sb). Shells B, L, and M have the normal order for B_{zz}, B_{xy}, and B_{xz}, but the magnitudes of the anomalies are too large to be explained by the respective $\lvert F_\Delta(\mathbf{r}_l)\rvert^2$ for the three donors. Shell F [V(Sb) is considered to belong to shell F] is the most anomalous of all, exhibiting the largest donor differences of all the observed shells—furthermore the B_{zz} components are the largest of all the observed shells; the B_{xy} components are singularly strongly negative; the B_{xz} components are strongly inverted. These results suggest that the type of corrections discussed in Sec. II C may explain some of these anomalous features since the corrections are strongly shell dependent and will be different for the different dipole-dipole constants. These seem to be just the features shown in the data in HM I.

III. CONSEQUENCES OF WAVE-FUNCTION ADMIXTURE FROM SUBSIDIARY MINIMA

A. Hyperfine Interaction with Donor Nucleus

From the Fermi contact hyperfine interaction one can infer the magnitude of the wave-function density $\lvert\psi_b(\mathbf{r}_l)\rvert^2$ at a given lattice site. The value $\lvert\psi(0)\rvert^2$ at the donor nucleus has been obtained from the donor hyperfine splitting.[10,12] For the P donor Kohn and Luttinger[4] noted that the effective-mass value

$$\lvert\psi(0)\rvert^2_{\text{eff mass}}=6\eta/\pi a^{*3}$$

was approximately a factor of 10 too small. Their approach was to increase substantially the envelope function $F_j(r)$ by solving the radial equation as a differential equation using the experimentally observed $1s$-A_1 state ionization energy, thus producing a sharply peaked Whittaker function and a cutoff radius ($R_c\sim$a Wigner-Seitz cell radius) between interior and exterior regions. An alternative approach is to mix in wave function (in phase) from more of the BZ than just the six Δ_1 minima. One has already achieved a factor of 6 over that of a single minimum having the same a^*. [n degenerate nonoverlapping minima characterized by isotropic $1s$ radii a_i^* will have

$$\lvert\psi(0)\rvert^2=\sum_{i=1}^{n}(1/\pi a_i^{*3})\eta_i,$$

where account has been taken of the $\lvert u_{k_i}(0)\rvert^2$ for different symmetry-point minima.] Equation (18) gives the correction factor for the contribution of subsidiary minima at L_1, K_1, and U_1. For $\mathbf{r}_l=0$ this factor is

$$N_{A_1}^{-1}\{1+\tfrac{4}{3}(a_\Delta^*/a_L^*)^{3/2}\beta_L+2(a_\Delta^*/a_K^*)^{3/2}\beta_K+4(a_\Delta^*/a_U^*)^{3/2}\beta_U\}^2. \quad (24)$$

The potential $U(r)$, including central-cell corrections, is attractive, the matrix elements $\langle A_{1j}\lvert U(r)\rvert A_{1-\Delta_1}\rangle$ are negative, and the α's and β's are positive. A crude guess of $\beta_L=\beta_K=\beta_U\sim0.1$, assuming equal Bohr radii for all the minima, gives a correction factor of about 3 with the largest contribution coming from the lower-symmetry K_1 and U_1 regions because of the greater number of valleys associated with these points.

Employing this correction we have calculated $\lvert\psi(0)\rvert^2$ for As, P, and Sb using the b^* method for the radial envelope function, namely,

$$F(r)=(1/\pi b^{*3})^{1/2}\exp(-r/b^*),$$

where $b^*=na^*$ and $n=(E_0/E_{1s-A_1})^{1/2}$. n is a quantitative measure[51] of the deviation of the ground-state energy from the effective-mass value E_0. As an approximation this same radial envelope function is used for all valleys. A justification for the use of the b^* envelope function is given in Sec. IV and Appendix A.

TABLE III. Valley interference factors (for equal spherical envelope functions).

Class	Lattice site	ENDOR shell	I_Δ $(k_0/k_m=0.875)$	I_L	I_K	I_U
4 ⟨001⟩ Axes	(0, 0, 4)	A^{12}	2.707	−4	2	4
	(0, 0, 8)	K^{11}	2.000	4	−2	−4
	(0, 0, 12)		1.293	−4	2	4
	(0, 0, 16)		1.000	4	6	12
3 ⟨111⟩ Axes	(1, 1, 1)	E^{12}	0.585	1.414	0.879	0
	(3, 3, 3)		−1.670	−1.414	5.121	0
	(4, 4, 4)		2.121	−4	0	0
	(5, 5, 5)		2.430	−1.414	5.121	0
	(7, 7, 7)		−2.940	1.414	0.879	0
	(8, 8, 8)		0.000	4	6	12
	(9, 9, 9)		2.940	1.414	0.879	0
2 {110} Plane	(2, 2, 0)		−0.840	0	−1.828	−3.656
	(4, 4, 0)	B^{12}	2.414	4	0	0
	(6, 6, 0)		0.234	0	3.828	7.656
	(8, 8, 0)		1.000	4	−2	−4
	(10, 10, 0)		1.766	0	3.828	7.656
	(14, 14, 0)		2.840	0	−1.828	−3.656
	(2, 2, 4)		−1.133	0	1	2
	(2, 2, 8)		−1.840	0	3.828	7.656
	(2, 2, 12)		−2.547	0	1	2
	(4, 4, 8)		1.414	4	0	0
	(8, 8, 4)		0.707	−4	2	4
	(1, 1, 3)		−0.167	−1.414	−1.121	0
	(1, 1, 5)	Q^{16}	1.220	−1.414	1.707	0
	(1, 1, 9)		1.370	1.414	−0.293	0
	(3, 3, 1)		−0.919	1.414	0.293	0
	(3, 3, 7)		−2.094	1.414	3.121	0
	(3, 3, 11)		−1.994	−1.414	−1.707	0
	(5, 5, 1)		1.855	1.414	3.121	0
	(5, 5, 9)		2.640	1.414	0.293	0
	(7, 7, 1)		−1.765	1.414	−0.293	0
	(7, 7, 3)		−2.517	−1.414	1.707	0
	(7, 7, 11)		−2.790	−1.414	−1.121	0
	(9, 9, 1)		2.155	1.414	−0.293	0
	(9, 9, 5)		2.790	−1.414	−1.121	0
	(11, 11, 3)		−2.217	−1.414	−1.707	0
	(11, 11, 7)		−2.640	1.414	0.293	0
1 Unique	(0, 4, 8)		1.707	−4	−2	−4
	(1, 5, 9)		2.005	−1.414	−0.293	0
	(3, 7, 11)		−2.367	1.414	−1.707	0

Table II compares the various calculated values of $|\psi(0)|^2$ with the experimental values inferred from the donor hyperfine splittings.[12] The calculated values given are the effective-mass value, the b^* value, and the b^* value multiplied by the correction factor in Eq. (24). This latter value is designated b^*-SM. Two different sets of β constants determined by fitting the ENDOR shell $a(\mathbf{r}_l)$ values were employed (see Table V below). The results indicate $|\psi(0)|^2_{b^*\text{-}SM}$ is in reasonable agreement for P but is much too small for As and Sb. However, if one multiplies $|\psi(0)|^2_{b^*\text{-}SM}$ by the correction factor $|\psi(0)|^2_{\text{atom-As,Sb}}/|\psi(0)|^2_{\text{atom-P}}\sim 2.5$ employed previously[4] to account for the strong change of $u_k(r)$ for As and Sb in the central cell,[52] the resulting As and Sb values [designated $(b^*\text{-}SM)_{\text{corr}}$ in Table II] are in much better agreement with the data. Table II clearly indicates that the second set of β's ($a_U^*=0.63a^*$) yield better agreement with experiment, the calculated values being 6, 9, and 28% too small for P, As, and Sb, respectively. Although the calculated values are somewhat too small, the agreement is reasonable and, significantly, the correct donor dependence of $|\psi(0)|^2$ has been obtained and the cutoff-radius problem (required for the Whittaker function) has been avoided. The admixture (in phase) of additional wave function from interior critical points of the

lowest conduction band will further increase the calculated $|\psi(0)|^2$, as will an increase in $F_j(0)$ for any of the valleys considered.

An additional interesting feature is that an arbitrary admixture of wave function from the U_1 "valleys" increases $|\psi(0)|^2$ *but does not increase* $|\psi(\mathbf{r}_l)|^2$ *for the* (1, 1, 1) *lattice site*, because the wave function from the square face of the BZ (XUW) can only contribute to the even-integer sites (see the I_U factors in Table III). By treating U_1 as a minimum the wave-function corrections from this region of the BZ have probably been underestimated. An increase in m_U* [flattening of $E(\mathbf{k})$] decreases a_U*, thus increasing $F_U(0)$ and $|\psi(0)|^2$. On the other hand, employing the Whittaker function for $F_\Delta(r)$ produces the unfortunate result of increasing some of the $a(\mathbf{r}_l)$ values too much for small $\mathbf{r}_l$ [see the (1, 1, 1) and (0, 0, 4) site calculated values in Table V].

B. Fermi Contact Constants for ENDOR Shells—Qualitative

To obtain a qualitative understanding of the corrections to $|\psi(\mathbf{r}_l)|^2$ from the subsidiary minima for specific lattice sites, we need only consider the magnitude and signs of the different valley interference factors I_Δ, I_L, I_K, and I_U. These are shown in Table III for a group of lattice sites which are thought to be potential measured ENDOR shells. For simplicity, the $F_j(\mathbf{r})$ are all assumed spherical with the same radial dependence, hence the $F_j(r)$ factors drop out of Eqs. (21a)–(21d). I_Δ is given at $k_0/k_{\max}=0.875$. For quantitative calculations the anisotropies of the various $F_j(\mathbf{r})$ must be considered.

Table III suggests substantially increased $a(\mathbf{r}_l)$ values for sites (2, 2, 0), (4, 4, 0), (6, 6, 0), (10, 10, 0), (5, 5, 1), (5, 5, 5), (4, 4, 8), and (8, 8, 8). It suggests substantially decreased $a(\mathbf{r}_l)$ values for sites $(\bar{3}, \bar{3}, \bar{3})$, (4, 4, 4), $(\bar{3}, \bar{3}, \bar{7})$, (2, 2, 8), and (0, 4, 8). Smaller increases are expected for sites (1, 1, 1), $(\bar{1}, \bar{1}, \bar{3})$, $(\bar{3}, \bar{3}, \bar{1}\bar{1})$, (5, 5, 9), $(\bar{7}, \bar{7}, \bar{1}\bar{1})$, (9, 9, 9), and $(\bar{1}\bar{1}, \bar{1}\bar{1}, \bar{3})$, while small decreases are expected for sites $(\bar{7}, \bar{7}, \bar{7})$, (3, 3, 1), (9, 9, 5), $(\bar{1}\bar{1}, \bar{1}\bar{1}, \bar{7})$, (2, 2, 4), (2, 2, 12), and (1, 5, 9). For shells like (1, 1, 5), $(\bar{7}, \bar{7}, \bar{3})$, (0, 0, 4), and (0, 0, 8) the correction to $a(\mathbf{r}_l)$ can be either positive or negative depending on the relative magnitudes of the coefficients β_L, β_K, and β_U. These positive and negative corrections are just what is needed to explain the donor anomalies observed in the data. The β's are expected to be largest for As, intermediate for P, and smallest for Sb. For the case of a large negative correction, the correction would be largest for As, intermediate for P, and smallest for Sb, possibly leading to an inverted order of the Fermi contact constants. A striking example of this is shell X [$\frac{1}{2}a(\mathbf{r}_l)=$ 242, 317, and 437 kHz for As, P, and Sb, respectively] which belongs to the {110}-plane class of shells. On this basis lattice sites $(\bar{3}, \bar{3}, \bar{7})$ and (2, 2, 8) would appear to be good candidates for shell X.

We also note that lattice sites (0, 0, 4) and (0, 0, 8) should have corrections of opposite sign which are simply related. These sites have been matched to the observed ENDOR shells A and K, respectively. Shell A is partly anomalous in that $a(A)_{\mathrm{Sb}}>a(A)_{\mathrm{P}}$ while shell K was not found[11] in Sb implying $\frac{1}{2}a(K)_{\mathrm{Sb}}<420$ kHz. The increased positive correction to $a(A)_{\mathrm{Sb}}$ with respect to P is consistent with a large decrease of $a(K)_{\mathrm{Sb}}$ and may account for the reason shell K was not found in Sb. Table III also indicates why the donor anomaly (normal ordering) is larger for shell B [matched as (4, 4, 0)] than for shell A, even though it is further from the donor. Shell C has been identified[12,11] as belonging to the ⟨111⟩-axis class of shells. It has as large a normal donor anomaly as shell B and has a significantly larger $a(\mathbf{r}_l)$ value than any of the other ⟨111⟩-axis-class shells. In the previous analyses[12,14] of $a(\mathbf{r}_l)$ versus $k_0/k_{\max}$ there was no value of $k_0/k_{\max}$ between 0.8 and 0.9, where a single ⟨111⟩-axis-class shell had an $a(\mathbf{r}_l)$ value several times the magnitude of all the other ⟨111⟩-axis-class shells as indicated by the data. In particular, their analysis suggested the $(\bar{3}, \bar{3}, \bar{3})$, (4, 4, 4) [also $(\bar{4}, \bar{4}, \bar{4})$] and (5, 5, 5) sites should all have nearly the same $a(\mathbf{r}_l)$ values for $k_0/k_{\max}=0.875$. Table III suggests a possible explanation of this dilemma, since it indicates sizable negative corrections for the $(\bar{3}, \bar{3}, \bar{3})$ and (4, 4, 4) sites and a probable sizeable positive correction for the (5, 5, 5) site.

A comparison of the valley interference factors for shells located along different crystal directions indicates the corrections due to the L_1, K_1, and U_1 regions produce a channeling effect along the ⟨110⟩ axis. Whereas the corrections for the cubic ⟨001⟩-axis sites and for the ⟨111⟩-axis sites oscillate in sign [except for sites (0, 0, 16) and (8, 8, 8), where all the I's are in phase and large, as at the origin] with increasing $\mathbf{r}_l$, for the ⟨110⟩-axis sites the corrections are positive and large at (2, 2, 0), (4, 4, 0), (6, 6, 0), and (10, 10, 0), are small for (8, 8, 0), and are negative for (12, 12, 0) and (14, 14, 0). Thus the first four of five sites (those most likely to be measured) along the ⟨110⟩ axis have large positive corrections. Other shells near the ⟨110⟩ axis like (5, 5, 1), (9, 9, 1), and $(\bar{1}\bar{1}, \bar{1}\bar{1}, \bar{3})$ also show positive corrections [$(\bar{3}, \bar{3}, 1)$ and $(\bar{7}, \bar{7}, 1)$ are exceptions]. Site (5, 5, 1) shows a rather large positive correction and is an excellent candidate for one of the larger $a(\mathbf{r}_l)$ values observed for {110}-plane-class shells; for example, shell D.

Table III also indicates that certain even-integer sites like (2, 2, 4), (2, 2, 8), and (2, 2, 12) [also (4, 4, 4); however, (4, 4, 8) is an exception] all have negative corrections. (2, 2, 8) has the largest negative correction of any of the sites in Table III. These even-integer sites (n, n, m), n and $m\neq 0$, have inversion-related mates, sites ($\bar{n}$, $\bar{n}$, $\bar{m}$), which in principle[14,25] should have slightly different $a(\mathbf{r}_l)$ values. As noted in HM II, and also in HC, none of these even-integer inversion-related shells have been identified. The fact that almost

all of them have large negative corrections to $a(\mathbf{r}_l)$ from the subsidiary minima might be an explanation for this.

The I_U values shown in the table are zero for all odd-integer sites, which appears to be a special property of the square faces (XUW) of the BZ. This is still true when anisotropic envelope functions are considered, as long as the envelope functions are the same for points related by inversion about the X point. For the U_1 points this requirement is that $F_{Xyz}=F_{X\bar{y}\bar{z}}$, $F_{Xy\bar{z}}=F_{X\bar{y}z}$, etc. This is certainly a reasonable approximation since the predominant part of the single-valley $1s$ envelope function should be even. One can also observe this feature in Fig. 8 of Ref. 12, which shows $a(\mathbf{r}_l)$ plotted versus $k_0/k_{\max}$ for the six Δ_1 minima wave function. As $k_0/k_{\max}$ approaches 1, $a(\mathbf{r}_l)$ goes to zero for all the odd-integer lattice sites. A second feature of the I_U values is that the even-integer sites, neglecting anisotropies, have $I_U(n, n, m)=2I_K(n, n, m)$, which is a reflection of the two-to-one equivalence between U and K points in the BZ.

Many sites listed in Table III were not explicitly considered previously.[12,14] Other close sites have not been included in Table III. Because of the large $k_0/k_{\max}$ value occurring in I_Δ and the slow decrease of the radial envelope function, it is the interference that is the dominant factor in determining which sites are observed within a radius of order a^*. The experimental evidence[11,12] for this is very compelling. A convenient means of selecting the sites with a large value of I_Δ is shown in Fig. 3, which shows the argument $\frac{1}{2}\pi(k_0/k_{\max})n$ plotted versus n. The projection on the horizontal axis gives the cosine. For $k_0/k_{\max}=0.86$, the values of n which yield positive cosine values (ordered by decreasing cosine magnitude) are 0, 14, 9, 5, 4, 10, 13, 1; those which yield negative cosine values (ordered by decreasing cosine magnitude) are 7, 16, 2, 12, 11, 3, 6, 8. The favored positive integers[53] are 0, 9, 5, and 4 while the favored negative integers are 7, 2, 12, 11, and 3. In combining integers for a site (n, n, m), the largest values of I_Δ are usually obtained when n and m differ by 0, 4, or 8. Of the 20 largest values of I_Δ ($|I_\Delta|>1.84$) shown in Table III, four have n and m the same, nine have n and m differing by 4, and four differ by 8; one is site (1, 5, 9) [a member of the unique class (l, m, n)]; and there are two exceptions, sites (2, 2, 12) and (2, 2, 8). Combining values of n and m corresponding to positive and negative cosines leads to small values of I_Δ, which in most instances have $a(\mathbf{r}_l)$ values too small to be observed as distinct shells. Only sites (2, 2, 0) and (6, 6, 0), because of their large positive corrections due to the subsidiary minima, may have large enough $a(\mathbf{r}_l)$ values to be observed. Sites like $(1, 1, \bar{7})$, $(1, 1, \bar{1}\bar{1})$, (1, 1, 13), $(\bar{3}, \bar{3}, 5)$, $(\bar{3}, \bar{3}, 9)$, $(5, 5, \bar{3})$, $(5, 5, \bar{7})$, $(\bar{7}, \bar{7}, 5)$, $(9, 9, \bar{3})$, and $(9, 9, \bar{7})$ have been considered and the $a(\mathbf{r}_l)$ values will be too small, even including favorable subsidiary minima corrections, to be observed. Site $(1, 1, \bar{3})$, the third nearest neighbor, and site $(\bar{3}, \bar{3}, 1)$, the fifth nearest neighbor, will be explicitly considered as examples of sites close to the donor with small I_Δ values. Using the b^*-method $F(r)$ and neglecting subsidiary minima corrections, one calculates $a(\bar{1}, \bar{1}, \bar{3})\simeq 14$ kHz (site radius=4.5 Å), while for a distant site $(\bar{7}, \bar{7}, 1\bar{1})$ one finds $a(\bar{7}, \bar{7}, \bar{1}\bar{1})\simeq$ 772 kHz (site radius=20.1 Å). This is an indication of the strong interference effects present in the wave function, even with only the six Δ_1 minima.

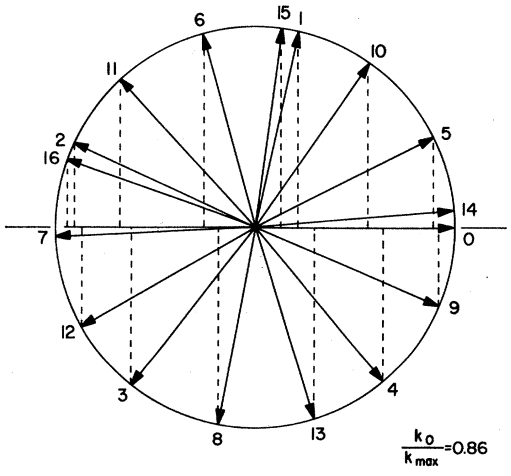

FIG. 3. Argument $(\pi/2)(k_0/k_{\max})n$ versus n for $n=0$–16. The projection on the horizontal axis gives the cosine, the magnitudes of which indicate which combination of integers (all even or all odd) for a lattice site (n, n, m) give large values of the interference factor I_Δ.

C. Uniaxial Stress-Induced Changes in $1s$-A_1 Wave Function

By measuring the change in the donor ground-state Fermi contact hyperfine interaction and the donor g-value shift with uniaxial stress, Wilson and Feher[33] determined the Δ_1 minimum g-tensor components $g_{\parallel}$ and $g_\perp$, in addition to reporting a "spin-resonance" value of the shear deformation potential constant $\Xi_u=11\pm1$ eV. More recently Watkins and Ham[54] have also reported a spin-resonance value $\Xi_u=11.4\pm1.1$ eV for the Li interstitial donor. These determinations are several eV higher than most values obtained by transport and optical techniques[55–59] in which the electron is a conduction electron within the Δ_1 minimum not subject to the impurity potential $U(r)$. Values of Ξ_u inferred from experiments involving the $1s$-A_1 donor state, which contains non-negligible wave-function admixtures from subsidiary valleys, may be effective values (which are donor dependent) rather than the true deformation potential for the Δ_1 minima.

The admixture of $1s$-A_1 wave function from subsidiary valleys changes the deformation potential by (1) changing the normalization of the wave function (reducing the Δ_1 minima component) and (2) the valley repopulation effect of the subsidiary valleys

(with their own deformation potential constants) caused by a uniaxial stress. A calculation for an ⟨001⟩ uniaxial stress employing the valley repopulation model for all valleys yields an expression for $\Xi_u)_{\Delta_1}$ in terms of an $\Xi_u)_{\text{eff}}$, presumably the measured value,[33] given by

$$\Xi_u)_{\Delta_1}=\Xi_u)_{\text{eff}}\left[\frac{1+4\beta_L/3+2\beta_K+4\beta_U}{1+2\beta_K\epsilon'^2+4\beta_U\epsilon''^2}\right]^{1/2}, \quad (25)$$

where ϵ' and ϵ'' are, respectively, $(\Xi_u/\Delta)_{K_1}/(\Xi_u/\Delta)_{\Delta_1}$ and $(\Xi_u/\Delta)_{U_1}/(\Xi_u/\Delta)_{\Delta_1}$ (Ξ_u/Δ is the coefficient appearing in the valley strain; see Ref. 33). The numerator of the correction factor contains the normalization change while the denominator contains the valley repopulation effect of the K_1 and U_1 valleys (the L_1 valleys are not split by a ⟨001⟩ uniaxial stress). Without specific knowledge of the deformation potentials and valley-orbit splittings for the K_1 and U_1 valleys (thus obtaining ϵ' and ϵ'') little can be concluded. If ϵ' and ϵ'' were somewhat greater than 1, Eq. (25) would suggest $\Xi_u)_{\Delta_1}<\Xi_u)_{\text{eff}}$. Equation (25) also implies that $\Xi_u)_{\text{eff}}$ should be donor dependent since $\Xi_u)_{\Delta_1}$ should be an intrinsic property of the pure silicon host lattice. In summary, caution should be exercised concerning Ξ_u values inferred from measurements on $1s$-A_1 donor states.

A second consequence of these subsidiary valley admixtures with their own valley repopulation effect will be corrections to the calculated i_d parameters reported in HC.[18] These corrections will include the same two contributions mentioned above. The valley repopulation correction factor [for an applied ⟨001⟩ uniaxial stress] of the K_1 and U_1 valleys has the form $c_{nm}(2\beta_K\epsilon'-4\beta_U\epsilon'')$ for even-integer sites and the form $c_{nm}\beta_K\epsilon'$ for odd-integer sites, where c_{nm} is a constant dependent on the lattice sites (n, n, m). Considering appropriate values of β_K and β_U (see Table V below) and $\epsilon'\sim\epsilon''$ one may expect the factor $(2\beta_K\epsilon'-4\beta_U\epsilon'')$ to be small. This may explain why the even-integer shells A, B, and K [matched as (0, 0, 4), (4, 4, 0), and (0, 0, 8), respectively] were readily fit in HC without serious corrections. These corrections will produce a donor-dependent i_d parameter. Detailed corrections to the i_d parameter will be given elsewhere.

A ⟨111⟩ uniaxial stress does not lift the degeneracy of the six Δ_1 minima, thus producing no repopulation effect. However, the introduction of L_1 and K_1 (the U_1 components on a single XUW BZ face can be lumped together,[60] the average effect resembling that of the Δ_1 minima) components will introduce a small valley repopulation effect, similar to that for the $1s$-A_1 state in Ge. Therefore a ⟨111⟩ uniaxial stress may be expected to produce small ENDOR shifts and splittings due *only* to the subsidiary valleys.[61]

Another consequence of the subsidiary valley admixtures is the possible splitting of the $1s$-T_2 states by a ⟨111⟩ uniaxial stress. The splitting of this triplet p-like state by a ⟨111⟩ uniaxial stress is allowed by symmetry but is not contained within the valley repopulation model based on only the six Δ_1 minima. The $1s$-T_2 states play a crucial role in the Orbach spin-lattice relaxation of the shallow donors.[62] An ⟨001⟩ uniaxial stress has been shown to quench the Orbach spin-lattice relaxation rate for As and P donors.[63] A much smaller quenching has also been observed[64] for a ⟨111⟩ uniaxial stress. One possible explanation of this small ⟨111⟩ effect is a small splitting of the $1s$-T_2 states caused by a valley repopulation effect of the subsidiary valleys.

D. Energy of Donor 1s States

The energy of the $1s$-A_1 state contains both single-valley and valley-valley interaction contributions [resulting from the matrix elements $\langle\psi_j \mid U(\mathbf{r}) \mid \psi_i\rangle$] and has the form

$$E_{1s-A_1}=-E_0+\langle F_\Delta \mid \delta U \mid F_\Delta\rangle-(4\Delta_a+\Delta_0)$$
$$-\alpha_L{}^2(E_{L_1}-E_{\Delta_1})-(\alpha_K{}^2+\alpha_U{}^2)(E_{K_1}-E_{\Delta_1}). \quad (26)$$

The effective-mass energy E_0 is given very closely by $m_\Delta{}^*e^4/2\hbar^2\epsilon_0{}^2$, and for $m_\Delta{}^*=0.322m$[65] and $\epsilon_0=11.7$,[66] one finds $E_0=32.0$ meV, a value slightly larger than the Kohn-Luttinger value. The second term represents the single-valley correction from $\delta U(\mathbf{r})$, while the third term represents the coupling between the degenerate Δ_1 minima[67] (Δ_a is the coupling between adjacent minima on different axes; Δ_0 is the coupling between opposite minima on the same axis). The remaining terms represent the contributions, using second-order perturbation theory, from the subsidiary minima. The corresponding expressions for the $1s$-E and $1s$-T_2 (spin-orbit splitting neglected) states are

$$E_{1s-E}=-E_0+\langle F_\Delta \mid \delta U \mid F_\Delta\rangle+(2\Delta_a-\Delta_0)$$
$$-(\epsilon_K{}^2+\epsilon_U{}^2)(E_{K_1}-E_{\Delta_1}), \quad (27a)$$

$$E_{1s-T_2}=-E_0+\langle F_\Delta \mid \delta U \mid F_\Delta\rangle+\Delta_0-\tau_L{}^2(E_{L_1}-E_{\Delta_1})$$
$$-(\tau_K{}^2+\tau_U{}^2)(E_{K_1}-E_{\Delta_1}). \quad (27b)$$

It is difficult to reliably estimate the magnitudes of the various terms because of the difficulty in obtaining a reliable expression for δU. One might use the best set of β's obtained from fitting the ENDOR data to obtain the α's [from Eqs. (20)], then estimate the energy differences $(E_{K_1}-E_{\Delta_1})$ and $(E_{L_1}-E_{\Delta_1})$, and obtain an estimate of the second-order contributions to E_{1s-A_1}. However, the second-order terms are actually related to the first-order valley-valley coupling terms Δ_a and Δ_0 because the α's contain sums of matrix elements of the type $\langle\psi_j(\mathbf{r}) \mid U(r) \mid F_x u_{k_0}(r)e^{ik_0x}\rangle$ which are similar to the matrix elements for Δ_a and Δ_0. An attempt has been made to calculate all these matrix elements employing a realistic impurity potential in Sec. IV D.

Qualitatively, considering the results in Sec. IV D, it can be demonstrated that it is the valley-valley coupling terms, both from the Δ_1 minima and in second order from the subsidiary minima, which are responsible for

nearly all of the energy correction to the $1s$-A_1 state. In fact, the single-valley correction is small (≤ 1.6 meV). The importance of the second-order terms from the subsidiary minima relative to $(4\Delta_a+\Delta_0)$ should increase with the ionization energy deviation, i.e., should be most important for As and least important for Sb. The corrections to the $1s$-E and $1s$-T_2 states from the subsidiary minima will be very much smaller (ϵ's and τ's$\ll\alpha$'s) than for the $1s$-A_1 state and are probably negligible, except perhaps for Sb. It is more difficult to estimate the relative importance of the different correction terms in Eqs. (27a) and (27b), in part because of a small uncertainty in the value of E_0. Finally, even with $\delta U=0$ there will still be small donor-independent energy corrections from the valley-valley coupling terms. Therefore E_0, the effective-mass value for a single minimum, is not the true effective-mass value for a multivalley case.

IV. CALCULATION OF FERMI CONTACT CONSTANTS; MATCHING SITES WITH SPECIFIC ENDOR SHELLS

A. Procedure

Calculations of the Fermi contact constants $a(\mathbf{r}_l)$ for As, P, and Sb donors have been performed by computer for approximately 35 different lattice sites of the type (n, n, m). With a few exceptions the selected group of sites was chosen on the basis of favorable I_Δ's and/or favorable corrections within a radius of 25 Å. These calculations were made using Eq. (18) considering β_K, β_U, and β_L as parameters which can be found from the identified ENDOR shells or can be varied in a systematic manner to obtain the best over-all fit to the experimental data. In as much as Eq. (18) contains 15 different parameters a number of simplifying assumptions were made.

A_0 and k_0 were considered as parameters, but were only varied in a narrow range ($6.25<A_0<7.60$ MHz; $0.84<k_0/k_{\max}<0.90$) because of experimental knowledge[18,47] of these parameters. As a simplification the isotropic $1s$ radii for all the different minima were first chosen to be the same, namely $a_K^*=a_U^*=a_L^*=a_\Delta^*=19.2$ Å. This value was obtained from $a_\Delta^*=a_0\epsilon_0(m/m_\Delta^*)$ using the best values of ϵ_0 and m_Δ^* and it is slightly smaller than used previously. The calculated results exhibited some features suggesting a reduced a_U^* value would better fit the experimental results and several calculations were performed with reduced a_U^* values. This reduction is consistent with U_1 being a saddle point rather than a minimum. Anisotropic pancake effects on the various valley interference factors [see Eq. (21)] were initially neglected, but were then incorporated, first for the Δ_1 minima, next for the L_1 minima, and finally for the K_1 and U_1 "minima." The anisotropic portion of the envelope function can be written in the form

$$F_z)_{\text{anis}} = \frac{\exp[-(z^2/a_l^2)+(x^2/a_{t1}^2)+(y^2/a_{t2}^2)]^{1/2}}{\exp(-r/a^*)}, \quad (28)$$

where $a^*=(a_l a_{t1} a_{t2})^{1/3}$.[68] This is the same relationship as among the mass tensor components and the isotropic mass, namely, $m^*=(m_l m_{t1} m_{t2})^{1/3}$. The axes x, y, and z are the principal axes of the specific valley ellipsoid under consideration and are different for each type of minimum. The a^* values are determined from m^* using $a^*=a_0\kappa(m/m^*)$, while the different a_j are found from the mass tensor components (measured for the Δ_1 minima; calculated for the L_1 minima; estimated from the band-structure calculations for the K_1 and U_1 valleys) and the relationship of Lampert[69] between m_l/m_t and a_t/a_l which is shown in Fig. 4. The values of m_j and a_j used for the different minima are shown in Table IV.

Two different checks of the calculations were made by

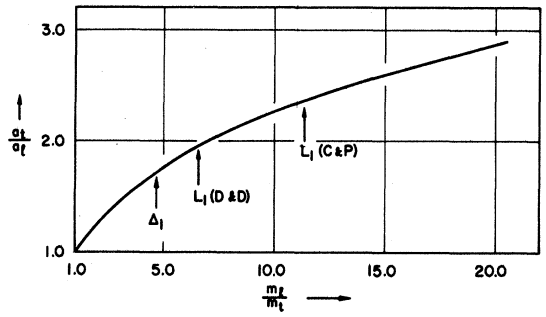

FIG. 4. Relationship between the anisotropic "pancake" radii ratio and the mass tensor components ratio for an ellipsoidal energy surface. This was calculated from the expression given by Lampert (Ref. 69). The Δ_1 value is obtained from cyclotron resonance values of the masses (Ref. 65). Two different calculated values of the masses at the L_1 point by Cardona and Pollak (Ref. 31) and Dresselhaus and Dresselhaus (Ref. 32) give calculated values for the radii ratio.

TABLE IV. Estimated masses and Bohr radii employed for the different subsidiary minima.[a]

Masses	L_1	K_1[b]	U_1[c]
m_l/m	1.81	0.596	0.488
m_{t1}/m	0.136	0.085	0.080
m_{t2}/m	0.136	0.596	0.852
m_j^*/m	0.322	0.322	0.510
Radii	Å	Å	Å
a_l	10.3	15.2	11.1
a_{t1}	25.8	30.5	18.3
a_{t2}	25.8	15.2	8.7
a_j^*	19.2	19.2	12.1

[a] These are the values used for the second b^*-SM values given in Table V, namely, for $a_U^*=0.63a^*$.

[b] For the K_1 "valley" t_1 is taken along the KW edge of the BZ while t_2 is taken along KL.

[c] For the U_1 "valley" t_1 is taken along the UW edge of the square face while t_2 is taken along $U\Sigma'X$.

comparing them with the experimental results. These quantitative checks were made with the following expressions:

$$f_i = n_i^{-1} \sum_l^{n_i} \left| \frac{a(\mathbf{r}_l)_{\text{calc}} - a(\mathbf{r}_l)_{\text{expt}}}{a(\mathbf{r}_l)_{\text{expt}}} \right| . \quad (29a)$$

and

$$f_{\text{total}} = \sum_l^{n_t} a(\mathbf{r}_l')_{\text{calc}} / \sum_l^{n_t} a(\mathbf{r}_l)_{\text{expt}} . \quad (29b)$$

The first quantity represents the average fractional deviation of calculated and experimental $a(\mathbf{r}_l)$ values for the lattice sites identified with ENDOR shells—either identified previously or identified on the basis of the new calculations. n_i is taken to be 14; however, this does not imply all these shells have been positively identified. The second quantity f_{total} is summed in the denominator over the experimentally measured shells (see HM I), 21 for As and P (shells U and W were excluded) and 19 for Sb [the AAA region in Sb was arbitrarily assigned two shells with $a(\mathbf{r}_l)/2 = 415$ kHz; however, there may be more shells in this region]. In the numerator the sum is over the 21 largest (19 largest for Sb) calculated values. Thus for a good fit f_i should be very small and f_{total} very close to 1. f_{total} is proportional to A_0, but is also a function of k_0, the β's, the pancake anisotropies in $F_j(\mathbf{r})$, and the type of envelope function employed. The introduction of a wave-function component lacking inversion symmetry may also affect f_{total} since it may introduce a positive bias by removing from consideration lattice sites where the correction is large and negative. f_{total} was found to decrease noticeably as $(a_t/a_l)_{A_1}$ was increased from 1.0 to 2.0, whereas f_{total} increased slightly as $(a_t/a_l)_{L_1}$ was increased from 1.0 to 2.5. For a given set of all the other parameters the value of A_0 was obtained by requiring f_{total} to be close to 1.

For the radial envelope function previous comparisons[12,14] have used the Whittaker function, which introduces a large enhancement of $F_j(\mathbf{r})$ for small r and requires the introduction of a cutoff radius. As already noted in Sec. III A it is possible, with the addition of the subsidiary minima, to greatly enhance $|\psi(0)|^2$ and thereby reasonably account for the values of $|\psi(0)|_{\text{expt}}^2$ obtained from the donor hyperfine interaction.[10,12] This eliminates the need for increasing $F_j(0)$ in the manner employed previously.[4] In addition, most of the energy correction to the $1s$-A_1 state results from valley-valley interactions and that the correction to the single-valley effective-mass energy from $\delta U(\mathbf{r})$ is small (see Sec. IV D). The large valley-valley interactions for the $1s$ states require the use of a coupled-valley Schrödinger equation.[70] This question is considered in Appendix A.

One can construct Schrödinger equations for functions which are various linear combinations of the single-valley $F_j(\mathbf{r})$. The equation with the totally symmetric linear combination has an eigenvalue E_{1s-A_1}, while the equations with other combinations of the $F_j(\mathbf{r})$, even and odd, have eigenvalues E_{1s-E} and E_{1s-T_2}. The spherical component of the envelope function $F_j(\mathbf{r})$ should be determined by the Schrödinger equation for the totally symmetric combination with eigenvalue E_{1s-A_1}. This argument leads directly to the b^* form of $F_j(r)$ given previously. The anisotropic components of the envelope functions result from solutions of the other coupled equations with eigenvalues E_{1s-E} and E_{1s-T_2}. For this reason we have used the uncorrected effective-mass radii a^*, etc., in Eq. (28).

This exponential form $F_j(\mathbf{r})$ is certainly an oversimplification for the radial wave function, yet the results discussed below suggest it is in much better agreement with the experimental results than the Whittaker function. The effects of $\delta U(\mathbf{r})$, considered on a single-valley basis, are small enough that they might be included by perturbation theory. For Sb the possibility of $U(\mathbf{r})$ being repulsive for small r ($1.5 < r < 4$ Å) suggests $F_j(r)$ is not simply exponential and may have a somewhat smaller value at the (2, 2, 0) site than given by the b^* form of $F_j(r)$ [see the Sb results for sites (2, 2, 0), (6, 6, 0), and (10, 10, 0) in Table V].

The procedure for obtaining the values of β_L, β_K, and β_U was the following. Taking the square root of Eq. (18) yields

$$3\left[\frac{a(\mathbf{r}_l)N_{A_1}}{A_0}\left(\frac{F_{a^*}(0)}{F_\Delta(\mathbf{r}_l)}\right)^2\right]^{1/2} = I_\Delta(\mathbf{r}_l) + \beta_K I_K(\mathbf{r}_l) + \beta_U I_U(\mathbf{r}_l) + \beta_L I_L(\mathbf{r}_l). \quad (30)$$

One inserts in Eq. (30) the experimental value $a(\mathbf{r}_l)$ for an identified ENDOR shell. The envelope functions and the $I_j(\mathbf{r}_l)$'s are readily calculated while A_0 is determined from the actual results and the use of the f_{total} check. The effect of N_{A_1} is small, but can be included by iteration. Thus one has a set of linear equations for all of the lattice sites that have been matched to specific experimental ENDOR shells reported in HM I. If we are given correct envelope functions for the different valleys, the right k_0, and the right pancake anisotropy parameters, and thus the correct $I_j(\mathbf{r}_l)$'s, then the overdetermined set of linear equations should be reasonably consistent with one another *provided* contributions from other critical points in the lowest conduction band, and also contributions from a noninversion component of the wave function, are unimportant. In practice, over-all excellent consistency is difficult to achieve and the reasons for the inconsistencies can be hard to isolate.

The following points were considered in selecting sites. (1) Sites should be used, if possible, where the corrections are large (I_K and I_U, and/or I_L large). (2) Sites where the corrections are primarily due to only one or two different type valleys are preferred to those where all three types of valleys make important corrections; for example, (0, 0, 4) and (0, 0, 8). (3)

TABLE V. Comparison of calculated and experimental values. (All hyperfine constants are in kHz.)

Site	Donor	Calculated $\frac{1}{2}\mid a(\mathbf{r}_l)\mid$ Whit.[b]	b^* [c]	b^*-SM[d] (1)	b^*-SM[e] (2)	B_{zz} b^*	Match[l]	Experimental[a] $\frac{1}{2}\mid a(\mathbf{r}_l)\mid$	B_{zz}	Shell
	As	5201	3334	3928	4032	96.4		3860	57.0	
(0, 0, 4)	P	4184	2728	3325	3316	78.8	√[f]	2981	41.4	*A*
	Sb	3684	2533	3150	3399	73.2		3101	46.0	
	As	927	926	747	611	97.5		758	16.0	
(0, 0, 8)	P	851	808	644	560	85.2	√[g]	663	14	*K*
	Sb	794	768	616	485	81.0		N.F.[h]	···	
	As	1051	259	625	667			642		
(1, 1, 1)	P	733	204	413	444	···	√[f]	270	···	*E*
	Sb	604	187	295	308			293		
	As	1485	1040	366	356					
$(\bar{3}, \bar{3}, \bar{3})$	P	1271	870	341	379	···				
	Sb	1149	812	409	492					
	As	917	1053	607	643			801		
(4, 4, 4)	P	839	905	646	644	···		689	···	*H*
	Sb	780	854	751	746			703		
	As	1089	1150	1722	1746			2037		
(5, 5, 5)	P	1055	1034	1492	1458	···	√	1649	···	*C*
	Sb	1004	967	1318	1236			1397		
	As	557	781	552	475			739		
$(\bar{7}, \bar{7}, \bar{7})$	P	595	730	568	505	···		598	···	*O*
	Sb	590	707	615	571			670		
	As		2	530	411			694		
(8, 8, 8)	P		2	332	253	···		739	···	*J*
	Sb		2	165	173			629		
	As		373	504	524			607		
(9, 9, 9)	P		367	472	487	···		612	···	*N*
	Sb		364	436	433			N.F.		
	As	578	340	1177	1165	173.0		1121	151.0	
(2, 2, 0)	P	450	273	841	803	138.8	√	840	116.4	*F*
	Sb	389	252	615	722	128.0		504	37.0	*V*
	As	2061	1852	2848	2878	−34.6		3000	−41.6	
(4, 4, 0)	P	1789	1560	2159	2213	−29.1	√[f]	2254	−34.0	*B*
	Sb	1627	1460	1793	1841	−27.2		1833	−28.6	
	As	90	37	717	720	−29.0		741	−14.6	
(6, 6, 0)	P	82	33	464	472	−25.6	√?	582	−11.2	*L*
	Sb	76	31	280	370	−24.4		425	−5.8	
	As		241	764	682	−15.5		777	−60.8	
(10, 10, 0)	P		232	621	566	−14.9	√?	612	−40.6	*M*
	Sb		229	482	485	−14.7		559	−37.2	
	As	680	481	555	564	−43.9		566	−48.0	
(1, 1, 5)	P	587	401	485	474	−36.6	√[i]	524	−40.2	*Q*
	Sb	533	376	456	433	−34.2		387	−36.0	

TABLE V (*Continued*)

Site	Donor	Whit.[b]	Calculated $\frac{1}{2}\mid a(\mathbf{r}_l)\mid$ b^* [c]	b^*-*SM*[d] (1)	b^*-*SM*[e] (2)	B_{zz} b^*	Match[f]	Experimental[a] $\frac{1}{2}\mid a(\mathbf{r}_l)\mid$	B_{zz}	Shell
	As	841	865	315	332	−24.2		242	40	
$(\bar{3},\bar{3},\bar{7})$	P	804	759	349	374	−21.2	√?	317	29.4	*X*
	Sb	760	720	442	480	−20.1		437	20.4	
	As		352	571	593	−2.6		696	−4.8	
$(\bar{3},\bar{3},\bar{1}\bar{1})$	P		328	489	502	−2.4		662	−6	*P*
	Sb		319	421	417	−2.3		629	−5.8	
	As	872	827	1594	1608	53.4		1292	4.2	
(5, 5, 1)	P	809	713	1236	1235	46.0	√?	1117	3.6	*D*
	Sb	756	675	990	961	43.5		1003	3.0	
	As		725	878	872	−0.6		806	7.0	
(5, 5, 9)	P		670	774	777	−0.5	√?	764	5.0	*G*
	Sb		647	708	706	−0.5		761	4.6	
	As		806	756	719	21.0		718	−20.4	
$(\bar{7},\bar{7},\bar{3})$	P		731	674	665	19.1	√?	685	−17.4	*I*
	Sb		705	648	656	18.4		643	−14.0	
	As		325	397	375	23.2		428	24.8	
(9, 9, 1)	P		307	357	344	21.8	√?	379	21.0	*R*
	Sb		300	329	318	21.3		332	15.0	
	As		502	346	362	1.0		364	0.0	
(9, 9, 5)	P		482	369	380	1.0		398	0.0	*T*
	Sb		474	409	412	1.0		N.F.	···	
	As		625	439	459	22.0		377	−5.4	
(2, 2, 12)	P		587	442	461	20.8		410	−5.4	*S*
	Sb		571	467	470	20.1		N.F.	···	
	As		274	576	526	30.2		338	···	
(4, 4, 8)	P		246	492	414	28.9		383	···	*U*
	Sb		236	351	323	27.6		N.F.		
	As		406	564	517	8.7				
$(\bar{7},\bar{7},\bar{1}\bar{1})$	P		398	520	482	8.5				
	Sb		392	473	439	8.4				
	As	853	570	268	193	149.0				
(2, 2, 4)	P	708	473	260	203	124.2				
	Sb	632	441	289	198	116.0				
	As	816	765	47	56	73.6				
(2, 2, 8)	P	771	673	95	108	64.7				
	Sb	727	640	183	135	61.6				
	As	537	348	164	168	55.6				
(3, 3, 1)	P	447	286	169	169	45.8				
	Sb	399	266	197	199	42.6				
	As		258	318	286	−25.1				
(1, 1, 9)	P		230	265	248	−22.3				
	Sb		219	236	227	−21.3				

TABLE V (*Continued*)

		Figure-of-Merit Results and Admixture Parameters									
		Whit.	b^*	b^*-*SM* (1)				b^*-*SM* (2)			
f_i	As	0.382[j]	0.545	0.081				0.105			
	P	0.507[j]	0.417	0.102				0.133			
	Sb	0.370[j]	0.338	0.084				0.105			
f_t	As	0.99[k]	0.843	0.990				0.978			
	P	1.03[k]	0.891	0.982				0.972			
	Sb	1.05[k]	0.941	1.003				1.017			
				β_K	β_U	β_L	N_{A_1}	β_K	β_U	β_L	N_{A_1}
	As	···	···	0.170	0.106	0.141	1.057	0.182	0.086	0.142	1.062
	P	···	···	0.146	0.085	0.098	1.037	0.146	0.072	0.106	1.039
	Sb	···	···	0.105	0.065	0.052	1.019	0.092	0.082	0.060	1.026

[a] Data from E. B. Hale and R. L. Mieher, Phys. Rev. **184,** 739 (1969).
[b] Whit. $-k_0/k_{max}=0.86$, $(a_t/a_l)\Delta_1=1.75$, $a_\Delta^*=21$ Å; these values are from computer results furnished by E. B. Hale; see also Figs. 5–7 in Ref. 14.
[c] $b^*-k_0/k_{max}=0.875$, $A_0=7.00$ MHz, $(a_t/a_l)_{\Delta 1}=1.75$, $a_\Delta^*=19.2$ Å.
[d] b^*-*SM* $k_0/k_{max}=0.875$, $A_0=7.20$ MHz, $(a_t/a_l)_{\Delta 1}=1.5$, $(a_t/a_l)_{L1}=$ (1) 2.25, $a_L^*=a_K^*=a_U^*=a_\Delta^*=19.2$ Å.
[e] b^*-*SM* $k_0/k_{max}=0.870$, $A_0=7.00$ MHz, $(a_t/a_l)_{\Delta 1}=1.5$, $(a_t/a_l)_{L1}=$ (2) 2.50, $(a_{t1}/a_l)_{K1}=2$, $(at_2/a_l)_{K1}=1$, $(a_{t1}/a_l)_{U1}=1.65$, $(a_{t2}/a_l)_{U1}=0.69$, $a_L^*=a_K^*=a_\Delta^*=19.2$ Å, $a_U^*=.63\,a_\Delta^*=12.1$ Å.
[f] G. Feher, Phys. Rev. **114,** 1219 (1959).
[g] E. B. Hale and R. L. Mieher, Phys. Rev. **184,** 751 (1969).
[h] N. F. indicates this shell was not found.
[i] E. B. Hale and T. G. Castner, Jr., Phys. Rev. B **1,** 4763 (1970).
[j] These values are based on only the seven positively identified ENDOR shells *A*, *B*, *C*, *E*, *F*, *K*, and *Q* because the Whit. calculations were not done for some of the lattice sites associated with tentatively identified ENDOR shells. Inclusion of shells *L*, *M*, and *X* will increase f_i.
[k] These values are estimates based on 15 lattice site calculated values and the 15 largest experimental values for each donor. Some of the omitted sites may have larger calculated $a(\mathbf{r}_l)$ values which will slightly increase the f_t values.
[l] $\surd$ indicates a positive identification. $\surd$? indicates a tentative identification.

Neither very close [for example, (1, 1, 1)] nor very distant sites should be selected: for the former, a lattice distortion (slightly different covalent radii for different donors) might affect $a(\mathbf{r}_l)$, while for the latter the pancake anisotropies can be large resulting in less reliable values of the $I_j(\mathbf{r}_l)$ in Eq. (30). (4) It is better to average over a number of matched site-ENDOR shells, particularly for the sites (n, n, m), n and $m\neq 0$, hopefully to diminish the effects of neglecting lack of inversion or a missing critical-point admixture to ψ. Site (4, 4, 0), identified as shell *B*, was selected because this site is the best-known site for determining β_L since the effect of the K_1 and U_1 valleys is small. Sites (2, 2, 0), (6, 6, 0), and (10, 10, 0), tentatively matched with ENDOR shells *F* [V(Sb)], *L*, and *M*, respectively, were averaged to yield an expression nearly independent of β_L which is a linear combination of β_U and β_K. Sites (1, 1, 5) (identified as shell *Q*), (5, 5, 5) (almost certainly shell *C* from Table III), and (5, 5, 1) and $(\bar{3}, \bar{3}, \bar{7})$ (tentatively identified as shell *D* and shell *X*, respectively) were used to form a linear combination of equations which yields a result nearly independent of β_L, thereby determining β_K. Except for Sb the sites (2, 2, 0), (6, 6, 0), and (10, 10, 0) exhibited reasonable consistency. Sites (1, 1, 5), (5, 5, 5), (5, 5, 1), and $(\bar{3}, \bar{3}, \bar{7})$ gave relatively poorer consistency with As the worst, P intermediate, and Sb the best with only small inconsistencies. (5, 5, 5) and $(\bar{3}, \bar{3}, \bar{7})$ seem to require much larger values of β_K than (5, 5, 1). The source of the discrepancy is unknown, but these sites can be affected significantly by a component of ψ lacking inversion symmetry, which will not affect the $(n, n, 0)$ or $(0, 0, m)$ sites.

B. Results

In Table V the calculated results for 28 lattice sites for two slightly different sets of β_L, β_K, and β_U (one set for $a_U^*=a_\Delta^*$, the second for $a_U^*=0.63a_\Delta^*$) are compared with the experimental values from HM I. Along with these are shown the calculated values based on the Whittaker $F_j(r)$ (from HM II) and the $b^*F_j(r)$ for just the six Δ_1 minima (β's equal zero). Also shown are the experimental and calculated values of B_{zz}, the latter based on Eq. (23a) assuming $J_1=J_2=33$ kHz, an average value of these integrals based on several identified shells. The checks ($\surd$) indicate positive identification of lattice sites with ENDOR shells from previous work[12,11] or this study while the checks with question marks indicate tentative identifications. The unidentified ENDOR shells are always given in the correct symmetry class (see HM I) but should not necessarily be associated with the calculated lattice site values to the left. Since lack of inversion symmetry (at the atomic nuclei—the argument applies only to even-integer sites) has not yet been considered, one has $a(\bar{n}, \bar{n}, \bar{m})=a(n, n, m)$; therefore the inversion-related sites [for example, $(\bar{4}, \bar{4}, \bar{4})$, $(\bar{2}, \bar{2}, \bar{1}\bar{2})$, etc.] have not been listed in the table. The experimental values, however, may include inversion-related pairs. One speculative possibility would relate lattice sites (4, 4, 4) and $(\bar{4}, \bar{4}, \bar{4})$ to ENDOR shells *H* and *O*, respectively, as discussed below.

Before discussing individual sites and shells, some qualitative comments on the over-all agreement should be made. The b^* values (without subsidiary minima) are too small for many well-identified shells like A, B, and E and they lead to much too small a value of f_{total}. The Whittaker function values are too large for some shells (A, K, E, and Q) and too small for others (B, C, D, and F), but a reasonable value of f_{total} is found. Both these sets have rather poor f_i values for the "identified" sites. Because of a substantial positive bias in the corrections, the b^*-SM calculated values have satisfactory values of f_{total}, in addition to having much smaller values of f_i, the agreement being close to 10% for the three donors. It also seems possible to explain some of the striking donor anomalies observed in the data. The agreement is sufficient to identify several new shells positively and some others tentatively. Nevertheless, the fit is clearly not an optimized fit and further refinement of the calculations with a finer grained variation of some of the parameters seems both probable and desirable since better agreement will then yield reliable information on the detailed shape of the lowest conduction band. We now consider in detail the agreement for specific lattice sites and the matched ENDOR shells, insofar as is possible.

(0, 0, 4) *and* (0, 0, 8) *Sites—Matched Previously with Shells* A[12] *and* K[11]

The agreement is apparently better for the first b^*-SM than the second, except that the second predicts the anomaly $a_{\text{Sb}}(0, 0, 4) > a_{\text{P}}(0, 0, 4)$ and also predicts a much smaller $a_{\text{Sb}}(0, 0, 8)$ (this shell was not found experimentally and should have $\frac{1}{2}a < 420$ kHz; it might be in the AAA region). The second b^*-SM (0, 0, 4) values are too large for three donors, and the (0, 0, 8) values are too small for two donors, indicating an incorrect balance between the L, the K, and U corrections, possibly because of incorrect anisotropic radii or too large a β_U.

(1, 1, 1) *Site—Matched Previously with Shell* E[12]

The agreement of As and Sb is excellent, while it is poor for P and thereby accounts for nearly one-half the contribution to f_i for P. This is not accounted for by the smaller covalent bond radius of P because a smaller radius for the (1, 1, 1) Si would increase the cosine thereby increasing $a(\mathbf{r}_l)$, making the agreement worse. A significant decrease of β_K and β_L would help but would worsen the agreement for many other shells.

(5, 5, 5) *Site—Matched as Shell* C

Although the calculated values are somewhat too small they are substantially larger than any other ⟨1, 1, 1⟩-axis-class site and the assignment with shell C is consistent with the small dipole-dipole constant as noted by Hale and Mieher.[18] The component of ψ lacking inversion symmetry might substantially improve the agreement as noted below.

Other ⟨1, 1, 1⟩*-Axis-Class Sites*

The agreement is sufficiently poor that no other shells can be matched with lattice sites. One possible reason is the neglect of the component of ψ lacking inversion symmetry and further discussion is reserved until after this is considered below.

(2, 2, 0) *Site—Matched as Shell* F [V(Sb)]

This site can be identified by its very large B_{zz} value (largest of all the shells) assuming the large contribution of the second term in Eq. (23a). The agreement of the $a(\mathbf{r}_l)$ values is good for As and P and somewhat worse for Sb. The agreement for Sb could be made much better by reducing β_U about 20% but this would make the agreement worse for sites (0, 0, 4), (6, 6, 0), and (10, 10, 0). Another possible explanation is the repulsive region of $U(r)$ for Sb [9] which might reduce $F_j(r)$ in the vicinity of (2, 2, 0). Considering the dipole-dipole constants[11] and the stress behavior,[16] there seems to be little doubt that V(Sb) should be associated with the very anomalous F shell.

(4, 4, 0) *Site—Matched Previously as Shell* B[12]

The agreement is satisfactory although all the values are somewhat too small.

(6, 6, 0) *and* (10, 10, 0) *Sites—Matched Tentatively as Shells* L *and* M*, Respectively*

These shells have patterns very similar to shell B characterized by negative B_{zz} values (shell M has the largest negative B_{zz} values of all the shells); they have sizeable B_{xy} values, and also have large donor anomalies with normal ordering. The very large corrections (see Table III) suggest (6, 6, 0) and (10, 10, 0) should be observed and shells L and M are the only promising candidates. The agreement of the b^*-SM values is reasonable and they indicate the larger donor anomaly for (6, 6, 0) thus suggesting (6, 6, 0) as L and (10, 10, 0) as M. This is not in agreement with the dipole-dipole calculations (neglecting SM corrections) which suggest the reverse assignment. The uniaxial stress behavior is the most anomalous of all the shells (see HC). These assignments await corrections to the dipole-dipole and piezo-hyperfine constants. There do not seem to be any other promising lattice sites for shells L and M.

(1, 1, 5) *Site—Matched Previously as Shell* Q

The agreement for this shell is reasonable although the calculated values are too small for P and too large for Sb. The reason for this is not understood.

($\bar{3}$, $\bar{3}$, $\bar{7}$) *Site—Matched Tentatively as Shell* X

Only this site gives reasonable agreement with the strongly inverted donor anomaly of shell X. Although

sites (2, 2, 4), (2, 2, 8), and (3, 3, 1) have substantial negative corrections, none of these sites give reasonable agreement. It is unlikely shell X is an even-integer site since there doesn't appear to be an inversion-related mate in the data. The (3, 3, 1)-site values exhibit too small an inverted donor anomaly and are too small in any case. However, the uncorrected B_{zz} value for the $(\bar{3}, \bar{3}, \bar{7})$ site is in poor agreement with shell X.

$(\bar{3}, \bar{3}, \bar{1}\bar{1})$ *Site—Unidentified; Shell P is a Possibility*

The calculations suggest this site should be observed. It should have a relatively small negative uncorrected B_{zz}, a negative i_d parameter, and a normal donor anomaly. Shell P has these characteristics; however, the calculated values are somewhat too small and the calculated donor anomaly is too large.

(5, 5, 1) *Site—Matched Tentatively as Shell D*

This assignment is troublesome because the dipole-dipole constant B_{zz} and the stress results are in poor agreement with this assignment. The calculated b^*-*SM* values are approximately correct although the calculated normal donor anomaly is too large. No other unmatched lattice site has large enough $a(\mathbf{r}_l)$ values to be a good candidate for shell D, although site (5, 5, 9) would be in better agreement with the small dipole-dipole constants and the small i_d parameter for shell D. Site (5, 5, 1) seems certain to have been measured and no other experimental shell besides D is a favorable candidate for site (5, 5, 1).

(5, 5, 9) *Site—Matched Tentatively as Shell G*

The calculated values show too large a normal donor anomaly; however, with respect to the uncorrected dipole-dipole constants and the uniaxial stress i_d parameter this assignment is excellent. Distant sites are much more sensitive to the mass anisotropies in the valleys, therefore some caution is required. It is highly probable this site has been measured. While shell D should not be ruled out completely, shells like I and P are not good candidates when one considers the dipole-dipole constants and the i_d parameters. Shell G is certainly the best choice at present.

$(\bar{7}, \bar{7}, \bar{3})$ *Site—Tentatively Matched as Shell I*

The $a(\mathbf{r}_l)$ values are in reasonable agreement with this assignment; however, the uncorrected dipole-dipole constants and uniaxial stress parameter i_d deviate somewhat. Shell P is also a possible candidate for this site.

$(\bar{7}, \bar{7}, \bar{1}\bar{1})$—*Unmatched*

The calculations, neglecting the noninversion component of ψ, suggest this shell might have been observed. It should have a small normal donor anomaly, a small positive B_{zz}, small B_{xy} and B_{xz} values, and a negative i_d value. While shell P should not be ruled out completely, it seems improbable that this distant site has been measured.

(4, 4, 8) *Site—Unmatched*

This site and its inversion-related mate should be considered as possible candidates for shells I and P (see the uniaxial stress i_d values in HC); however, this assignment is in poor agreement with the dipole-dipole constants. Were this assignment to be confirmed, then sites $(\bar{7}, \bar{7}, \bar{3})$ and $(\bar{3}, \bar{3}, \bar{1}\bar{1})$ would have to be eliminated from consideration, requiring strong unknown negative corrections for these sites. It seems more probable from the b^*-*SM* values of $a(\mathbf{r}_l)$ for (4, 4, 8), particularly the large donor anomaly, that site (4, 4, 8) should be eliminated from consideration, but this remains an open question.

(9, 9, 1) *Site—Matched Tentatively as Shell R*

This assignment seems very good although corrections are required to explain the uniaxial stress i_d values. The calculated b^*-*SM* values, including the magnitude of the donor anomaly, are in good agreement with the experimental values for shell R. The (7, 7, 1) site was also considered as a candidate for shell R, but it has a negative correction from the subsidiary minima and has calculated $a(\mathbf{r}_l)$ values which are substantially too small. It seems unlikely shell R could be matched to an even-integer site since there does not appear to be an inversion-related mate in the data.

(9, 9, 5) *and* (2, 2, 12) *Sites—Unmatched, but Tentatively Associated with Shells S, T, and U*

All of these shells exhibit inverted donor anomalies for As and P. They have not been found in Sb; however, there is a reasonable probability some of them are in the *AAA* region (see HM I). These lattice sites should have small dipole-dipole constants and small i_d values, which is consistent with the data in HM I and HC (the i_d of shell U was not measured). The uncorrected calculated i_d value is smaller for (9, 9, 5) than for (2, 2, 12) or its inversion-related mate $(\bar{2}, \bar{2}, \bar{1}\bar{2})$, which suggests it is a better candidate for the remarkable shell T which has $B_{zz}=0.0$ kHz and an $|\, i_d \,|<0.01$. Despite the lack of any positive identification, it is encouraging that the subsidiary minima corrections yield lattice sites with the right characteristics for these shells.

(2, 2, 4) *and* (2, 2, 8) *Sites—Not Expected To Have Been Measured*

The strong negative corrections for these sites and their inversion-related mates, particularly for (2, 2, 8), yield small $a(\mathbf{r}_l)$ values and suggest these sites have not been measured. The $a(\mathbf{r}_l)$ values for (2, 2, 8) have been reduced by factors of 15, 6.6, and 4 for As, P, and Sb, respectively, which indicates the importance of a small admixture of the numerous K_1 and U_1 valleys.

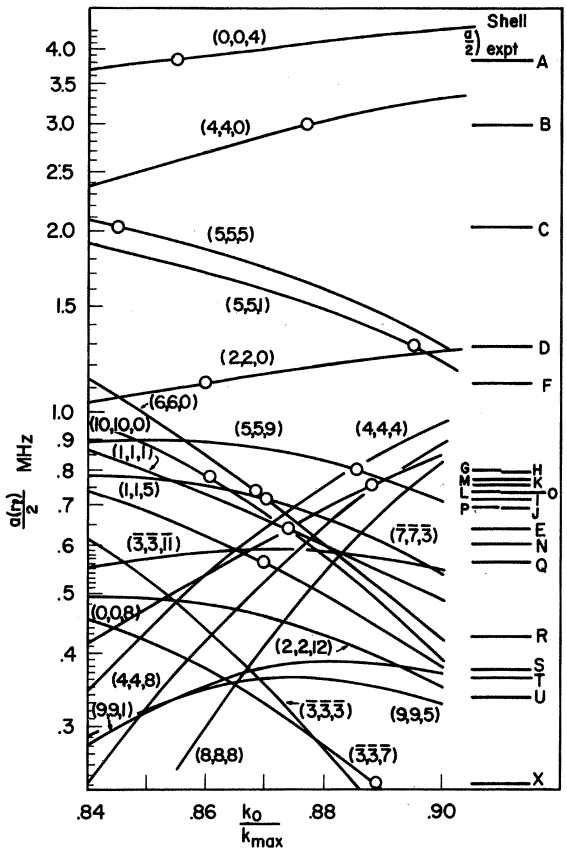

FIG. 5. The calculated Fermi contact constants versus k_0/k_{max} including the subsidiary minima corrections (but neglecting the noninversion contribution) from the L_1, K_1, and U_1 regions of the lowest conduction band [the β_j admixture coefficients used were the second set ($a_U^*=0.63a^*$) given in Table V]. The experimental values taken from Hale and Mieher (Ref. 11) are shown to the right. Matching circles were found for 13 of the positively and tentatively identified shells [the (9, 9, 1) site calculated values always remains below the shell R value]. While shells H and O were not considered tentatively identified in Table V, it is noted that they can be reasonably matched with lattice sites (4, 4, 4,) and $(\bar{4}, \bar{4}, \bar{4})$ but probably not with site $(\bar{3}, \bar{3}, \bar{3})$.

(1, 1, 9) *Site—Not Expected To Have Been Measured*

The small negative correction for this site yields $a(\mathbf{r}_l)$ values slightly below the continuum limits given in HM I. No measured shell has the appropriate dipole-dipole constants or uniaxial stress i_d to be a reasonable candidate for this site.

(3, 3, 1) *Site—Not Expected To Have Been Measured*

The calculated $a(\mathbf{r}_l)$ values of this site, which is close to the donor (fifth nearest neighbor), are substantially below the continuum limits because of the negative correction from the L_1 minima. The $(\bar{1}, \bar{1}, \bar{3})$ site (third nearest neighbor) has also been considered and has $a(\mathbf{r}_l)$ values well below the continuum limit.

Having incorporated corrections to $a(\mathbf{r}_l)$ from the subsidiary minima, it is of interest to fit the $a(\mathbf{r}_l, k_0/k_{max})$ values to the experimental data in order to check what spread of k_0 values occurs. Using the second set of β_L, β_K, and β_U ($a_U^*=0.63a^*$) given in Table V the values of $a(\mathbf{r}_l, k_0/k_{max})$ have been calculated and are shown for As in Fig. 5. Matching circles are obtained for 13 of the 14 "identified" shells [the calculated $a(\mathbf{r}_l, k_0/k_{max})$ values for site (9, 9, 1) were slightly too small to be matched with shell R]. These matching circles lead to a mean value $\langle k_0\rangle_{As}=0.872k_{max}$. A similar analysis for P (13 matching circles) and Sb (10 matching circles) yields mean values $\langle k_0\rangle_P=0.872k_{max}$ and $\langle k_0\rangle_{Sb}=0.866k_{max}$. An analysis of the over-all spread in k_0/k_{max} "fit values" indicates it is much smaller than the previous analyses[12,14] and suggests a value $k_0/k_{max}=0.87\pm0.01$. This is in good agreement with the value $k_0/k_{max}=0.86\pm0.02$ reported in HC (the value in HC would have been slightly higher had the calculated values of Δa been based on the b^* envelope function rather than the Whittaker function).

Inspection of Fig. 5 indicates the unmatched $\langle 111\rangle$-axis-class shells H and O are far better candidates for the (4, 4, 4) and $(\bar{4}, \bar{4}, \bar{4})$ sites than for the $(\bar{3}, \bar{3}, \bar{3})$ site. It should be emphasized that the results in Table V and in Fig. 5 have been based on a wave function that has inversion symmetry (with respect to the even-integer lattice sites). A wave-function component lacking inversion symmetry can introduce systematic deviations which will affect the results in Table V and Fig. 5.

C. Inversion Symmetry of ψ?

As noted previously[25,14] the $1s$-A_1–state donor wave function need not possess inversion symmetry. This feature does not result from the band structure because of the cubic symmetry (O_h^7 space group) of the diamond lattice. However, the donor possesses only T_d symmetry and $\delta U(\mathbf{r})$ can contain a tetrahedral potential $\delta U_t(r)=V_t xyz f(r)$. This potential has negligible effect on the valley-valley coupling because of its odd parity. However, in the single-valley Schrödinger equation [see Eq. (4)], it can be treated by perturbation theory. It admixes f function (satisfying the A_1 representation) from $n=4$ on to much higher n. This "tetrahedral" component of ψ will have the form

$$\psi_t=xyz\sum_{n=4}^{\infty}\frac{\langle nf\text{-}A_1\,|\,\delta U_t\,|\,1s\text{-}A_1\rangle}{(E_{1s-A_1}-E_n)}\times A_n L_{n+3}^{7}(\rho)\exp(-\rho/2), \quad (31)$$

where $L_{n+3}^{7}(\rho)$ is the associated Laguerre polynomial and A_n is a normalization constant for the nf function. The anisotropic mass tensor has been neglected and simple hydrogenic functions have been used in Eq. (31). The energy denominator is nearly constant for $n=4$ and larger. Because of very large Bohr radii of these f functions and the short range[71] of $\delta U_t(\mathbf{r})$, the matrix elements will decrease slowly with n and might be ap-

proximated by $\langle nf\text{-}A_1 \mid \delta U_t \mid 1s\text{-}A_1\rangle \sim V_0(1-\alpha)^{n-4}$ where $\alpha \ll 1$. The summation in Eq. (31) can be done approximately by employing a generating function[72] for the associated Laguerre polynomials leading to the approximate result

$$\psi_t \simeq Cxyz \exp(-r/\lambda), \tag{32}$$

where $\lambda \ll 4a^*$, the Bohr radius of the $4f$ state. The value of λ is difficult to determine and will depend on how rapidly the matrix elements decrease with n, i.e., on the value of α. Neglecting mass anisotropies, one obtains the same type of function for all the valleys, including the subsidiary valleys. With this f-function admixture, the correction to $a(\mathbf{r}_l)$ is readily estimated since ψ_t will factor out of each $F_j(r)$ term. The cross-term result can be shown to be[73]

$$\Delta a(\mathbf{r}_l)_i = C'(x_l y_l z_l / a^{*3}) \times [\exp(-\mathbf{r}_l/\lambda)/\exp(-\mathbf{r}_l/b^*)] a(\mathbf{r}_l). \tag{33}$$

Equation (33) can be employed to calculate $\Delta a(\mathbf{r}_l)_i$ if λ and the constant C' ($C' \propto V_t$) are known. For the estimates made here we set $\lambda = b^*$ and attempt to determine C' from the data for a set of tentatively identified inversion-related ENDOR shells. The set most likely to have been observed (identifiable partly on the basis of the symmetry class) is (4, 4, 4) and $(\bar{4}, \bar{4}, \bar{4})$. A careful consideration of all the unidentified $\langle 111\rangle$-axis-class shells indicates that only H and O give a plausible set of C' values [the same sign for all three donors and a reasonable donor dependence, in this case $C'(\mathrm{P}) > C'(\mathrm{As}) > C'(\mathrm{Sb})$]. The uncorrected dipole-dipole constant values [see HM I and Eq. (23b)] favor H as (4, 4, 4) and O as $(\bar{4}, \bar{4}, \bar{4})$. This assignment is also supported by the sign of the required corrections for a number of identified shells. Shells C and R require positive corrections while shell X requires a negative correction. Also sites $(\bar{7}, \bar{7}, \bar{7})$, $(\bar{3}, \bar{3}, \bar{3})$, and $(\bar{7}, \bar{7}, \bar{1}\bar{1})$ require negative corrections to be considered not observed. All of the above facts require C' to be positive [$\delta U_t(r)$ attractive, V_t negative] making $\Delta a(\mathbf{r}_l)_i$ positive [with respect to $a(\mathbf{r}_l)$] in the positive quadrant (n, n, m) and negative in the negative quadrant $(\bar{n}, \bar{n}, \bar{m})$.

Qualitatively the correction $[\Delta a(\mathbf{r}_l)/2]_i$ is largest for the more distant shells close to the $\langle 111\rangle$ axes which also have large values of $a(\mathbf{r}_l)$. These corrections have been calculated with Eq. (33) using shell-H and shell-O data to determine C'.

The effect of $[\Delta a(\mathbf{r}_l)/2]_i$ on all the sites is not an obvious over-all improvement. While the "identified" sites (5, 5, 5), (9, 9, 1), and $(\bar{3}, \bar{3}, \bar{7})$ are substantially improved the sites (5, 5, 9), $(\bar{7}, \bar{7}, \bar{3})$, and (9, 9, 5) are now in noticeably poorer agreement with the data. Although site $(\bar{7}, \bar{7}, \bar{1}\bar{1})$ is substantially decreased to near the continuum limits, site (4, 4, 8) is increased making it appear to be a measured shell, while site $(\bar{3}, \bar{3}, \bar{1}\bar{1})$ is decreased enough to make it a questionable choice for shell P. For the $\langle 111\rangle$-axis-class sites, $(\bar{3}, \bar{3}, \bar{3})$ and $(\bar{7}, \bar{7}, \bar{7})$ are still both slightly above the continuum limits in HM I, but there are no $\langle 111\rangle$-axis shells with values of $a(\mathbf{r}_l)/2$ this small. Site (9, 9, 9) is boosted substantially (too much), making it appear to be a measured shell. Shells J and N are both candidates (J is much the better candidate on the basis of the donor anomaly). Site $(\bar{8}, \bar{8}, \bar{8})$ is reduced below the continuum limits, however site (8, 8, 8) has a large enough $a(\mathbf{r}_l)/2$ value for As and P to be considered a measured shell. Shell N might be a possibility except the donor anomaly is wrong and site (8, 8, 8) is expected to have a much larger B_{xy} value, not considering corrections due to the subsidiary minima. If sites $(\bar{3}, \bar{3}, \bar{3})$ and $(\bar{7}, \bar{7}, \bar{7})$ can really be removed from consideration (this seems questionable for Sb) one has obtained more reasonable general agreement for the unidentified $\langle 111\rangle$-axis shells than before the noninversion component of ψ was considered. The observation of site (8, 8, 8) seems rather unlikely, but if confirmed would be a most remarkable indication of the importance of the subsidiary minima since the b^* value of $a(\mathbf{r}_l)/2$ for (8, 8, 8) is negligible (see Table V).

In summary, this addition of f function makes some improvement in the $\langle 111\rangle$-axis shells, thus supporting the tentative assignment of shells H and O to sites (4, 4, 4) and $(\bar{4}, \bar{4}, \bar{4})$, respectively. It suggests site (9, 9, 9) corresponds to a measured shell, but that sites $(\bar{3}, \bar{3}, \bar{3})$ and $(\bar{7}, \bar{7}, \bar{7})$ probably have not been measured. For the $\{110\}$-plane-class shells, the results are equivocal.

D. Valley-Valley Coupling Matrix Elements

Given a realistic donor potential $U(r)$ which takes account of the difference of the core potential of the donor atom and a silicon atom and also takes account of the dielectric shielding effects, then it is easy to estimate the valley-valley coupling matrix elements V_{jl} between the jth and lth valleys. Nara and Morita[74] have taken account of both these effects and find a spherical donor potential of the form

$$U(r) = \int \frac{[V_D(k) - V_{\mathrm{Si}}(k)] \exp(-i\mathbf{k}\cdot\mathbf{r})}{\epsilon(k)} \frac{d\mathbf{k}}{(2\pi)^3}, \tag{34}$$

noting that the anisotropy in $\epsilon(\mathbf{k})$ was shown to be small[26] and the isotropic component of $\epsilon(\mathbf{k})$ can be written[74] as

$$[\epsilon(k)]^{-1} = \frac{Ak^2}{k^2+\alpha^2} + \frac{Bk^2}{k^2+\beta^2} + \epsilon_0^{-1} \frac{\gamma^2}{k^2+\gamma^2}. \tag{35}$$

The coefficients A, B, α, β, and γ have been calculated by Nara[26]; however, we note that these constants are sensitive to detailed knowledge of the band structure and should not be considered accurately known. The form of $V_D(k) - V_{\mathrm{Si}}(k)$ used by Nara and Morita[74]

was

$$V_D(k)-V_{\mathrm{Si}}(k)=-4\pi e^2\left[\frac{1}{k^2}+\frac{Z_D-5}{k^2+\sigma_D{}^2}-\frac{Z_{\mathrm{Si}}-4}{k^2+\sigma_{\mathrm{Si}}{}^2}\right], \tag{36}$$

where the core potential of an n-fold ionized free ion was taken to have the form

$$[n+(Z_j-n)\exp(-\sigma_j r)](-e^2/r),$$

where Z_j is the Z of the atom and σ_j is an effective screening constant. Within this approximation one finds $U(r)$ to be of the form

$$U(r)=(-e^2/r)[\epsilon_0{}^{-1}+a_v\exp(-\alpha r)+b_v\exp(-\beta r)$$
$$+c_v\exp(-\gamma r)+d_v\exp(-\sigma_D r)-e_v\exp(-\sigma_{\mathrm{Si}} r)], \tag{37}$$

in which the coefficients are given by

$$a_v=A\left\{1-\alpha^2\left[\frac{(Z_D-5)}{\sigma_D{}^2-\alpha^2}-\frac{(Z_{\mathrm{Si}}-4)}{\sigma_{\mathrm{Si}}{}^2-\alpha^2}\right]\right\}, \tag{38a}$$

$$b_v=B\left\{1-\beta^2\left[\frac{(Z_D-5)}{\sigma_D{}^2-\beta^2}-\frac{(Z_{\mathrm{Si}}-4)}{\sigma_{\mathrm{Si}}{}^2-\beta^2}\right]\right\}, \tag{38b}$$

$$c_v=\epsilon_0{}^{-1}\left\{\gamma^2\left[\frac{(Z_D-5)}{\sigma_D{}^2-\gamma^2}-\frac{(Z_{\mathrm{Si}}-4)}{\sigma_{\mathrm{Si}}{}^2-\gamma^2}\right]-1\right\}, \tag{38c}$$

$$d_v=\left\{\frac{A\sigma_D{}^2}{\sigma_D{}^2-\alpha^2}+\frac{B\sigma_D{}^2}{\sigma_D{}^2-\beta^2}-\frac{\gamma^2}{\epsilon_0(\sigma_D{}^2-\gamma^2)}\right\}(Z_D-5), \tag{38d}$$

$$e_v=\left\{\frac{A\sigma_{\mathrm{Si}}{}^2}{\sigma_{\mathrm{Si}}{}^2-\alpha^2}+\frac{B\sigma_{\mathrm{Si}}{}^2}{\sigma_{\mathrm{Si}}{}^2-\beta^2}-\frac{\gamma^2}{\epsilon_0(\sigma_{\mathrm{Si}}{}^2-\gamma^2)}\right\}(Z_{\mathrm{Si}}-4). \tag{38e}$$

As $r\to 0$, $U(r)\to -e^2(Z_D-Z_{\mathrm{Si}})/r$ as required. In this potential the terms a_v, b_v, and c_v result from the dielectric screening effects and can lead to a net repulsive contribution to $U(r)$ which is largest for Sb. Nara and Morita[74] observed that for large enough r such that the core terms (d_v and e_v) are negligible, Sb can have a repulsive $U(r)$ for a small range of r; however, this behavior is very sensitive to the screening constants employed.[75]

The matrix element V_{jl} between the jth and lth valleys is

$$V_{jl}=\int F_l(r)u_{\mathbf{k}_l}(\mathbf{r})^*\exp(-i\mathbf{k}_l\cdot\mathbf{r})U(r)$$
$$\times F_j(r)u_{\mathbf{k}_j}(\mathbf{r})\exp(i\mathbf{k}_j\cdot\mathbf{r})d\tau$$
$$\approx\int F_l(r)F_j(r)\exp[i(\mathbf{k}_j-\mathbf{k}_l)\cdot\mathbf{r}]U(r)d\tau$$
$$+\int_{\text{central cell}}(u_{\mathbf{k}_l}{}^*u_{\mathbf{k}_j}-1)F_lF_j$$
$$\times\exp[i(\mathbf{k}_j-\mathbf{k}_l)\cdot\mathbf{r}]U(r)d\tau, \tag{39}$$

where the usual approximation of averaging over $u_{\mathbf{k}}(\mathbf{r})$ has been made. If we neglect the central-cell correction term and also recognize that the principal contribution to V_{jl} results from the short-range portion of $U(r)$, it is an excellent approximation to neglect the anisotropic part of $F_j(\mathbf{r})$ [we use here the uncorrected a^* form of $F_j(r)$ for both valleys]. After performing the angular integration we find

$$V_{jl}=\frac{4}{a^{*3}}\int_0^\infty\exp\left(-\frac{2r}{a^*}\right)U(r)\frac{\sin(|\mathbf{k}_j-\mathbf{k}_l|r)}{|\mathbf{k}_j-\mathbf{k}_l|}r\,dr. \tag{40}$$

Qualitatively, for large $|\mathbf{k}_j-\mathbf{k}_l|$ it is only the very-short-range part of $U(r)$ which contributes appreciably to V_{jl} while for small $|\mathbf{k}_j-\mathbf{k}_l|$ a much larger portion of $U(r)$ contributes to V_{jl}. Based on shielding constants determined from Herman-Skillman atomic potentials[76] and on the dielectric coefficients from Nara and Morita[74] V_{jl} versus $|\mathbf{k}_j-\mathbf{k}_l|/k_{\max}$ has been calculated and the results are shown in Fig. 6. For very small

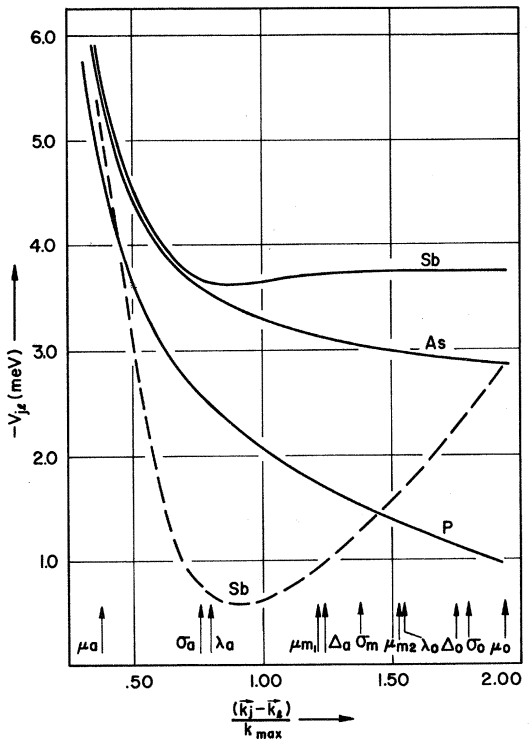

FIG. 6. Valley-valley coupling matrix elements calculated from Eq. (46) neglecting the central-cell correction term employing the potential in Eq. (44) with screening coefficients obtained from Herman-Skillman atomic potentials (Ref. 76). Though shown as smooth curves, the matrix elements are only between the valleys of the lowest conduction band, which are separated by discrete values of $|\mathbf{k}_j-\mathbf{k}_l|$. The various values of $|\mathbf{k}_j-\mathbf{k}_l|$ which give the various matrix elements (defined in Appendix A) between a particular Δ_1 valley and the other valleys are indicated above the lower scale. The dashed curve for Sb indicates the form of V_{jl} curve consistent with the empirical values β_L, β_K, and β_U obtained from fitting the Sb ENDOR shells.

$|\mathbf{k}_j-\mathbf{k}_l|$, the donor dependence is small and the largest contribution to V_{jl} results from $-e^2/\epsilon_0 r$, while for large $|\mathbf{k}_j-\mathbf{k}_l|$, V_{jl} is largest for Sb and smallest for P, thereby demonstrating the role of the core portion of $U(r)$. One can pick off Fig. 6 the $V(|\mathbf{k}_j-\mathbf{k}_l|)$ for the coupling between a Δ_1 valley and all the respective L_1, K_1, and U_1 valleys. In this manner the matrix elements $\langle A_{1-K_1}|U(r)|A_{1-\Delta_1}\rangle$, $\langle A_{1-L_1}|U(r)|A_{1-\Delta_1}\rangle$, and $\langle A_{1-U_1}|U(r)|A_{1-\Delta_1}\rangle$ (see Appendix A) are determined and are, respectively, -20.6, -15.2, and -47.8 meV for P. The central-cell term will tend to increase the magnitude of these matrix elements. Because of the lack of specific knowledge of $u_{L_1}(r_l)$, $u_{K_1}(r_l)$, and $u_{U_1}(r_l)$, it is difficult to make more than crude estimates of the α's from the β's, and hence of the energy gaps $E_{K_1}-E_{\Delta_1}$ and $E_{L_1}-E_{\Delta_1}$. These estimates indicate the energy gaps should be small, in the range 0.3–0.5 eV. This is smaller than most of the band calculations[26–32] predict although the $\mathbf{k}\cdot\mathbf{p}$ calculations of Cardona and Pollak[31] give values in this range. The pseudopotential calculations, except those of Kane,[30] predict energy gaps approximately a factor of 2 larger than these estimates. The magnitudes of the matrix elements $\langle A_{1-j}|U(\mathbf{r})|A_{1-\Delta_1}\rangle$ are the right order of magnitude to account for the magnitude of the admixture coefficients, the α's and the β's, and indicates the effectiveness of the potential in coupling the low-lying valleys. We reemphasize it is only the $1s$-A_1 state (where all the individual valley-valley coupling matrix elements add) that strongly exhibits the effect of the valley-valley coupling.

From Fig. 6 the Δ_1-Δ_1 valley interactions yield $(4\Delta_a+\Delta_0)=15.5$, 7.9, and 18.5 meV for As, P, and Sb, respectively. The As and P results clearly indicate these quantities are too small to account for all the energy deviation of the $1s$-A_1 state. By setting $\mathbf{k}_j=\mathbf{k}_l$ and subtracting $-e^2/\epsilon_0 r$ from $U(r)$, we obtain from Eq. (40) the single-valley correction $\langle F_\Delta(r)|\delta U(r)|F_\Delta(r)\rangle$ which for the above parameters is -1.6, -1.0, and -1.6 meV for As, P, and Sb, respectively. This is a very small fraction of the energy correction to the $1s$-A_1 state. The second-order energy corrections in Eq. (26) from the subsidiary minima can only be roughly estimated because of the conversion problem between the α's and the β's. An estimate based on $u_{K_1}(\mathbf{r}_l)=u_{L_1}(\mathbf{r}_l)=u_{U_1}(\mathbf{r}_l)=2u_{\Delta_1}(\mathbf{r}_l)$ and energy gaps $E_{K_1}-E_{\Delta_1}=E_{L_1}-E_{\Delta_1}=0.4$ eV yields second-order corrections of -12, -8, and -5 meV for As, P, and Sb, respectively. Thus the valley-valley coupling between the Δ_1 minima themselves and the subsidiary minima can readily account for all the energy deviation of the $1s$-A_1 donor state.

The principal problem regarding the valley-valley coupling matrix elements in Fig. 6 is the large overestimate of these matrix elements for Sb.[77] The reason for this is thought to be the inadequate description of the potential $V_{\mathrm{Sb}}(k)$ by a single screening constant—the potential $U(r)$ for Sb ($1.5<r<4$ Å) is not well described by Eq. (37). The problem is not solved by the argument of Nara and Morita[74] that with increased Z_D the coefficient a_v becomes more negative leading to a more repulsive $U(r)$ for $1.5<r<4.0$ Å, because Bi has a substantially larger value of both E_{1s-A_1} and $|\psi(0)|^2$ than As, and therefore the V_{jl} curve for Bi should be higher than for As. Sb seems to be the truly anomalous donor and the results suggest a very delicate balance of the terms in $U(r)$ which would produce the dashed curve $V_{jl}(|\mathbf{k}_j-\mathbf{k}_l|)$ shown in Fig. 6 which is required to account for the smaller β_K and β_L and the larger β_U of Sb relative to P. Although the matrix elements are very sensitive to the dielectric coefficients (particularly α), a change in these coefficients changes the $V_{jl}(|\mathbf{k}_j-\mathbf{k}_l|)$ curves proportionately for all the donors and would not account for the anomalous behavior of Sb.

V. EXTENSION TO DEEP DONOR

It is of interest to extend the subsidiary valley corrections approach to a donor with a significantly larger binding energy which still resides in T_d symmetry. Bi is the next more tightly bound shallow donor ($E_{1s-A_1}=-70$ meV) but no ENDOR data on this donor exist. The double donor S^+ [$Z=2$, $U(r)=-2e^2/\epsilon_0 r+\delta U(r)$] has been studied extensively and a detailed ENDOR study by Ludwig[25] has given hyperfine tensors for eight shells. Ludwig attempted to use the Kohn-Luttinger theory to explain the data, but found the agreement was poor, and was able to identify only one measured shell. The nearest-neighbor site (1, 1, 1) was identified with the largest $a(\mathbf{r}_l)$ value (largest of all eight shells) because of its symmetry pattern and its enormous dipole-dipole constant B_{xy}. Since the (1, 1, 1) site has the largest $a(\mathbf{r}_l)$ value, the wave function for this deep donor differs qualitatively from that for the shallow donors discussed above. The significantly stronger potential should greatly increase the coupling between the valleys.

The effective-mass energy for S^+ will be $-Z^2E_0\simeq-128$ meV, and the Bohr radius will be $a^*/Z=9.60$ Å. Using the binding energy (0.52 eV) employed by Ludwig, we find $n=0.50$ and $b^*_{S^+}=na^*_{S^+}=4.80$ Å (the b^* envelope function with these parameters was that employed by Ludwig). With the $a^*_{S^+}$ envelope function one can readily calculate the valley-valley coupling matrix elements V_{jl} using an appropriate screening constant σ_D for S^+. From these V_{jl} one obtains the matrix elements $\langle A_{1-j}|U(r)|A_{1-\Delta_1}\rangle$ and scales the β_j's for S^+ from those for P using the relationship

$$\beta_{j-S^+}=\left(\frac{\langle A_{1-j}|U(r)|A_{1-\Delta_1}\rangle_{S^+}}{\langle A_{1-j}|U(r)|A_{1-\Delta_1}\rangle_P}\right)\beta_{j-P}.$$

This yields for S^+ the values $\beta_L=0.890$, $\beta_K=1.240$, and $\beta_U=0.683$. Most of this substantial increase results from the eightfold increase of $(1/a^{*3})$ in Eq. (40). The S^+ core potential is only slightly stronger than that for P, but is much weaker than that for As and Sb. The

TABLE VI. Comparison of calculated and experimental Fermi contact constants for the substitutional S^+ donor.[a]

Site	Calculated $a(\mathbf{r}_l)/2$ values				Experimental[b]			
	b^*	b^*-SM[c]	b^*-SM[c]	b^*-SM[c]	$a(\mathbf{r}_l)/2$	B_{zz}	B_{xy}	$\lvert B_{xz}\rvert$
(1, 1, 1)	3.29	17.9	16.3	14.9	16.35	...[d]	12.0	B_{xy}
$(\bar{3}, \bar{3}, \bar{3})$	3.76	2.45	2.23	2.04	4.54	...	0.54	B_{xy}
(4, 4, 4)	1.95	0.12	0.05	0.03				
(5, 5, 5)	1.10	1.83	1.67	1.53	1.46	...	0.02	B_{xy}
(8, 8, 8)	0.001	0.20	0.21	0.21	0.68		0.10	B_{xy}
(0, 0, 4)	18.20	1.38	3.70	5.00	1.03	0.08	$\lvert 0.09\rvert$	...[d]
(2, 2, 0)	2.88	6.32	11.72	14.30	4.18	0.37	0.35	0.72
(4, 4, 0)	5.40	7.14	6.79	6.40				
(1, 1, 3)	0.11	5.80	5.28	4.83	1.92	0.53	0.28	0.35
(5, 5, 1)	1.42	4.24	3.86	3.53	2.39	0.03	−0.07	0.04
β_U	0	0	0.30	0.45				
N_{A_1}	1	5.0	5.5	6.0				

[a] All values in MHz.
[b] G. W. Ludwig, Phys. Rev. **137**, 1520 (1965).
[c] $\beta_L = 0.890$ and $\beta_K = 1.240$.
[d] ... indicates this value is required to be zero by symmetry.

overlap between valleys has also increased by more than an order of magnitude (see Appendix B) and $a_0(\mathbf{k}-\mathbf{k}_j)$ falls off much more slowly away from the minimum $\mathbf{k}_j$. While the L_1 and K_1 valleys are still far enough away in $\mathbf{k}$ space to be considered isolated valleys, it is now questionable whether the U_1 "saddle-point" region can be separated from the Δ_1 valleys. For this reason the calculations presented below are for several reduced values of β_U, including $\beta_U = 0$.

Values of $a(\mathbf{r}_l)$ are calculated for substitutional S^+ using Eq. (18), setting $k_0 = 0.87k_{\max}$, $A_0 = 56$ MHz (the eightfold increase results from the $1/a^{*3}$ factor), and employing the b^* envelope function. The choice of N_{A_1} is difficult because of the substantially increased valley-valley overlap and because linear terms in the α_M from overlap can now make a noticeable contribution to N_{A_1}. The choice of N_{A_1} has been dictated both by the estimates based on expression in Sec. II and the value of f_{total} (this latter check suggests a value of N_{A_1} in the range 5–6). The results for the b^* and three b^*-SM values are compared with the experimental $a/2$ values taken from Ludwig's study[25] in Table VI.

Qualitatively the b^*-SM values improve the over-all agreement in several respects: (1) The (1, 1, 1) site has the largest value of $a(\mathbf{r}_l)$; (2) the (0, 0, 4) site value is substantially reduced, remaining smaller than three of the {110}-plane sites for most of the range of β_U. Quantitatively, the results are much less reliable than for the shallow donors for several reasons: First, the values of α_L and α_K are now comparable to one and the use of perturbation theory is questionable; secondly, the Δ_1-U_1 region of $\mathbf{k}$ space has not been treated properly; finally, comparable qualitative agreement can also be obtained for S^+ in the tetrahedral interstitial site. From Table VI it is tempting to assign tentatively the third largest ⟨111⟩-axis shell ($a/2 = 1.46$ MHz) with the very small dipole-dipole constant B_{xy} to site (5, 5, 5), in analogy with shell C for the shallow donor case. This should be regarded as speculative until the corrections to the dipole-dipole constants are considered, since the subsidiary minima admixtures are so large. However, these corrections may be small since the B_{xy} component for shell C exhibits very little donor dependence.

For the S^+ donor the largest contribution to $|\psi(\mathbf{r}_l)|^2$ for sites (1, 1, 1), $(\bar{3}, \bar{3}, \bar{3})$, and (5, 5, 5) is no longer from the Δ_1 minima but is from the subsidiary minima. For site $(\bar{3}, \bar{3}, \bar{3})$ the major contribution to $a/2$ is from the K_1 valleys and negative corrections result from the Δ_1 and L_1 valleys—just the reverse of the shallow-donor case.

The admixture of wave function from other bands to the S^+ wave function has been suggested by Ham (see Ref. 25). Ham notes the Δ_2' band is a prime candidate because it is close in energy to Δ_1 and is coupled by $U(\mathbf{r})$. Previous discussion[41] has suggested the Δ_2' band is the extension of the Δ_1 band on an extended-zone scheme, and might thus be considered a higher-energy portion of the Δ_1 minimum valley. The S^+ donor would certainly be expected to have a very much larger admixture of Δ_2' band wave function than the shallow donors. Nevertheless, this Δ_2' band admixture will affect the interference characteristics of ψ much less than comparable amounts of wave-function admixture from other regions of the Brillouin zone (BZ). Wave-function admixture from a substantial portion of the BZ in ample amounts has the effect of greatly reducing the interference in $|\psi(\mathbf{r}_l)|^2$—in agreement with what appears to happen for S^+. While admixtures from other bands, particularly the Δ_2' band, seem likely, we suggest the lowest conduction band, with corrections from the subsidiary valleys and

as yet undetermined interior critical points, contributes the major portion of the S^+ donor $1s$-A_1 wave function.

VI. DISCUSSION AND CONCLUSIONS

What is the three-dimensional appearance of the wave-function density $|\psi(\mathbf{r}_l)|^2$ inferred from the Fermi contact constants? To what extent does the $1s$-A_1-state wave function reflect the tetrahedral symmetry of the silicon atoms surrounding the donor? These questions are best answered by considering the identified sites, the tentatively identified sites, and other possible lattice sites that may have been measured. These are shown in Fig. 7, which shows the sites in one of the six {110} planes (we recall from HM I that no unique class shells were measured above the continuum limits; thus all the measured lattice sites lie in these six {110} planes and each individual {110} plane contains all the measured sites). Figure 7 suggests channelling of $|\psi(\mathbf{r}_l)|^2$ along the ⟨110⟩ axis. Four sites have been identified or tentatively identified along this axis and large wave-function density extends further along this axis than along the cubic axes. Two sites have been positively identified along the positive ⟨111⟩ axis, site

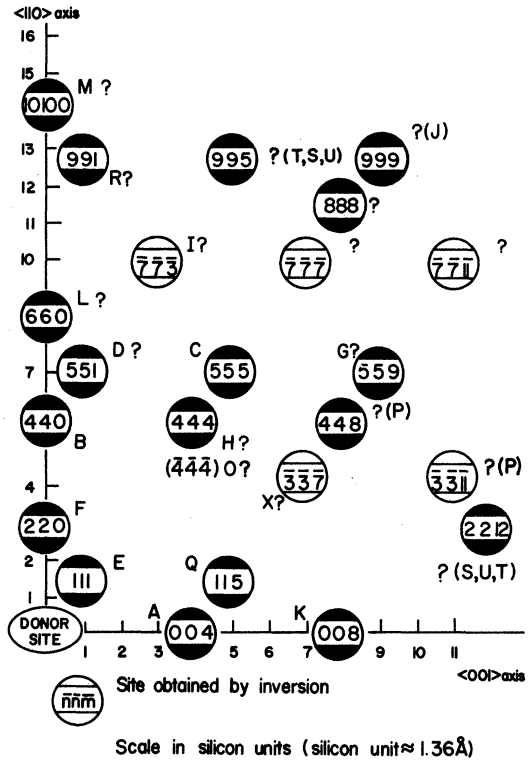

FIG. 7. Matching of the observed ENDOR shells with the lattice sites employing the calculated Fermi contact constants. The letter of an observed shell (see Hale and Mieher, Ref. 11) adjacent to a lattice site indicates a positive identification. A letter followed by a question mark indicates a tentative identification. A question mark followed by a letter or letters in parentheses suggests possible candidates for a particular site. A question mark alone indicates no favorable ENDOR shell for that site.

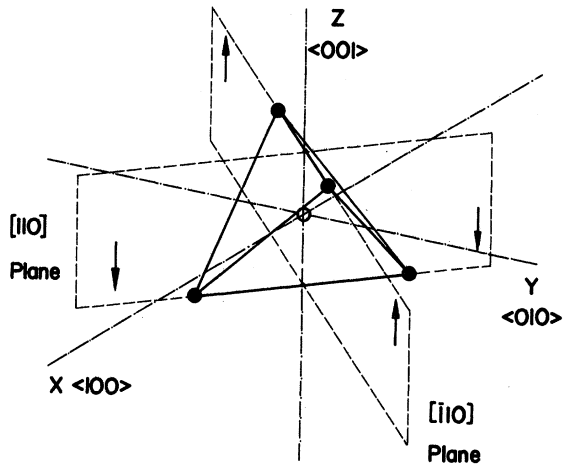

FIG. 8. The tetrahedron of the four nearest-neighbor silicon atoms surrounding the donor and two of the six reflection planes (vertical reflection planes in the T_d point group) which bisect the tetrahedron. In the [1̄10] plane the wave-function density is greater on the positive half of the plane. In the [110] plane the wave-function density is greater on the negative Z half of the plane.

(4, 4, 4) is tentatively matched with shell H, site (9, 9, 9) is a candidate for shell J, and site (8, 8, 8) has not been ruled out of consideration. Along the negative ⟨111⟩ axis site $(\bar{4}, \bar{4}, \bar{4})$ is tentatively matched with shell O, while sites $(\bar{3}, \bar{3}, \bar{3})$ and $(\bar{7}, \bar{7}, \bar{7})$ have almost been ruled out of consideration due to large negative corrections. Thus there is some evidence for channeling along the positive ⟨111⟩ axis. This preferential channeling along the positive ⟨111⟩ axis results partly from the subsidiary minima corrections and partly from the component of the wave function lacking inversion symmetry.

Another way of considering the wave-function density is to look at only the odd-integer sites in the [1̄10] plane since they are situated unsymmetrically with respect to the ⟨110⟩ axis which divides the [1̄10] plane into two halves (the sites repeat and are identical above and below the ⟨001⟩ axis). How many odd-integer sites on each half of the [1̄10] plane have been measured? On the right-hand half (positive quadrant), sites (1, 1, 1), (1, 1, 5), and (5, 5, 5) have been positively matched with ENDOR shells; sites (5, 5, 1), (5, 5, 9), and (9, 9, 1) have been tentatively matched; and sites (9, 9, 5) and (9, 9, 9) are candidates for measured shells. On the left-hand half, no sites have been positively matched; sites $(\bar{3}, \bar{3}, \bar{7})$ and $(\bar{7}, \bar{7}, \bar{3})$ have been tentatively matched; site $(\bar{3}, \bar{3}, \bar{11})$ is a candidate for a measured shell [sites $(\bar{3}, \bar{3}, \bar{3})$, $(\bar{7}, \bar{7}, \bar{7})$, and $(\bar{7}, \bar{7}, \bar{11})$ might be considered marginal candidates for measured shells]. Inspection of the $a(\mathbf{r}_l)$ values for these odd-integer sites in Table V indicates the possible measured $a(\mathbf{r}_l)$ values are noticeably larger (and also more numerous) on the right half of the [1̄10] plane. This indicates a higher probability for the donor elec-

tron to be on the right half of the $[\bar{1}10]$ plane than on the left half. The preference for the positive $\langle 111\rangle$ axis is in agreement with this conclusion.

When all six $\{110\}$ planes are considered this tendency for the electron to spend more time on the half of a specific $\{110\}$ plane containing the (1, 1, 1) nearest neighbors is a definite indication of the tetrahedral appearance of $|\psi(\mathbf{r}_l)|^2$. Figure 8 shows the tetrahedron of the four nearest neighbors surrounding the donor and two $\{110\}$ planes which intersect at right angles. In the $[110]$ plane the wave-function density is greater for negative Z [in the direction of the two (1, 1, 1) neighbors in this plane], while in the $[\bar{1}10]$ plane the wave-function density is greater for positive Z. The behavior is the same for the other four $\{110\}$ planes. This conclusion of the tetrahedral nature of $|\psi(\mathbf{r}_l)|^2$ is still true if one neglects the component of ψ lacking inversion symmetry; however, this component does enhance the effect. The regions of large wave-function density then consist of six intersecting sheets, namely, the six $\{110\}$ planes, with the donor residing at the common intersection of all six planes.

If the subsidiary minima corrections are neglected [see the b^* values of $a(\mathbf{r}_l)/2$ in Table V], there is still some tendency for the odd-integer sites to have larger values of $a(\mathbf{r}_l)$ in the positive quadrant (see Fig. 7) than in the negative quadrant. This reflects the position of the Δ_1 minima. For $k_0/k_{\max}=1$ all the odd-integer sites have $|\psi(\mathbf{r}_l)|^2=0$, while for $k_0/k_{\max}=0.5$ the values of $\cos(k_0x_l)$ are equal $\pm\sqrt{\frac{1}{2}}$ for all the odd-integer sites and there is no tendency for the interference factor I_Δ to be larger more often on the right or left half of the $[\bar{1}10]$ plane in Fig. 7. Thus the position of the Δ_1 minima themselves produces some tendency for $|\psi(\mathbf{r}_l)|^2$ to reflect the tetrahedral symmetry. Since it is the positions of the neighboring atoms and the resulting periodic potential which determines the band structure, it is not surprising that the weakly bound shallow-donor wave function reflects the tetrahedral symmetry. Nevertheless, this is the first reported evidence known to the author which indicates that the $1s$-A_1 wave function for the shallow donors really does exhibit tetrahedral symmetry.

One should also note that the effects discussed above reflect the fact that the unpaired electron shows a pronounced tendency to go in directions with a higher density of atoms since it can lower its energy by staying closer to the potential of the atoms.

How much has the Kohn-Luttinger wave function really been modified by the addition of the subsidiary minima components? This can be estimated from the normalization constant N_{A_1} (the unresolved conversion from the β's to the α's makes an accurate determination of N_{A_1} difficult). Since overlap between the valleys is small for the shallow donors N_{A_1} has the form given in Sec. II and $1/N_{A_1}$ represents the fraction of time the unpaired electron spends in the Δ_1 valleys. This is estimated to be larger than 94% for As, 96% for P, and 97% for Sb. The fractional time spent in all the other valleys is less than 6, 4, and 3% for As, P, and Sb, respectively. The reasons why these corrections are so important for the Fermi contact constants are (1) the large number of minima associated with the L, K, and U points yielding large interference factors I_L, I_K, and I_U for certain lattice sites; (2) the probable increased s component of the periodic function $u_k(r)$ at these points; (3) the complex interference pattern of the combination of different valleys, often leading to large corrections at sites where the six Δ_1 minima wave function is small; (4) the corrections are added linearly in amplitude and the result is squared in obtaining $a(\mathbf{r}_l)$. Thus relatively small corrections to the Kohn-Luttinger wave function can lead to major corrections in $a(\mathbf{r}_l)$.

It has been noted previously[14] that donor-dependent central-cell effects should only extend a distance the order of a Wigner-Seitz radius. The correction potential $\delta U(\mathbf{r})$ may extend somewhat beyond the Wigner-Seitz radius as indicated by the results of Nara and Morita[74]; however, the important large portion of $\delta U(\mathbf{r})$ is in the donor core region. The admixture of wave function from the subsidiary valleys is accomplished primarily by the short-range stronger portion of $U(\mathbf{r})$. *However, the effects of this admixture are revealed at large distances from the donor*, the extent depending on the Bohr radii a_j^* associated with the envelope functions $F_j(\mathbf{r})$ associated with the different subsidiary valleys. Consequently, distant lattice sites like (5, 5, 9), $(\bar{3}, \bar{3}, \bar{1}\bar{1})$, (8, 8, 8), (10, 10, 0), and (9, 9, 9) experience substantial corrections due to the subsidiary valleys even though they are well outside the range of the strong central-cell potential. It is precisely this long-range effect of the subsidiary-minimum corrections which accounts for the fact that approximately half of the ENDOR shells observed in HM I exhibit donor anomalies.

The treatment of the K_1 and U_1 regions in this work as minima, while incorrect in a rigorous sense, has allowed one to simply introduce wave functions from these portions of the BZ into the donor $1s$-A_1 wave function. The results indicate a substantially improved fit between the calculated and experimental Fermi contact constants of the identified ENDOR shells. This strongly supports the assertion that the donor $1s$-A_1 wave function contains non-negligible components from these low-energy regions of the lowest conduction band.

The evidence presented in this paper indicates the identification of a large number of ENDOR shells for a bound electron in a periodic solid can potentially yield a significant amount of information on the conduction band of that solid. An immediate question is whether the approach used in this paper can be extended to other solids. Grachev, Deigen, and Pekar[78] have used the method of Kohn-Luttinger to attempt to obtain information from the extensive F-center ENDOR

data[79] on the conduction-band minima in KCl and NaF. Their conclusion that the conduction-band minima in KCl and NaF may lie on the cubic ⟨100⟩ axes is in question because of the difficulty in correctly identifying some of the distant F-center ENDOR shells, and perhaps also because they did not consider contributions to the F-center wave function from subsidiary energy valleys of the conduction band or from other bands. The binding energy of the F center is approximately 50 times that of shallow donors, but the conduction-band–valence-band gap is only of the order of ten times larger than in silicon, and the width of the conduction band is only slightly larger than in silicon. This suggests that the relatively stronger potential of the F center, compared with that for the shallow donors in silicon, may couple the different valleys in the alkali-halide conduction bands much more strongly than for the case of the shallow donors. This in part may account for the fact that there is relatively little interference in the F-center wave function because the wave function is composed of a large portion of the BZ. Nevertheless, the successful identification of a substantial number of F-center ENDOR shells along different crystal axes could provide substantial information on the band structure of the alkali halides, provided the theory of the hyperfine tensor components correctly accounts for the topological features of the conduction band and neighboring bands of symmetry such that they are admixed into the F-center wave function by the impurity potential.

The principal conclusions of this paper are as follows.

(1) The admixture of wave function (configuration mixing) from the L_1 valleys, the K_1 valleys, and the U_1 "saddle-point" region of the lowest conduction band in silicon significantly improves the wave function of the shallow donors by improving the fit of the calculated Fermi contact constants with the experimental ENDOR shells. The improved fit is good enough to positively identify two new shells (C and F) and to suggest the tentative identification of nine other shells (D, G, H, I, L, M, O, R, and X) (the confirmation of these tentative identifications rests on making corrections to the hyperfine tensor dipole-dipole constants and to the piezo-hyperfine constants, in addition to further refinement of the Fermi contact calculations). The matching of the positively identified and tentatively identified shells with calculated values of $a(\mathbf{r}_l)$ versus $k_0/k_{\max}$ leads to a value $k_0/k_{\max}=0.87\pm0.01$ for the position of the Δ_1 minima—slightly larger than previously reported values.

(2) The admixture of wave function from the subsidiary minima changes the interference pattern of the donor wave function substantially and gives an adequate explanation of the many donor anomalies observed in the experimental data, accounting for both the large normal donor anomalies and the unusual inverted anomalies (shell X being the most important example). Large negative corrections for a number of previously promising lattice sites [(2, 2, 4), ($\bar{2}$, $\bar{2}$, $\bar{4}$), (2, 2, 8), ($\bar{2}$, $\bar{2}$, $\bar{8}$), (3, 3, 1), ($\bar{3}$, $\bar{3}$, $\bar{3}$), and ($\bar{7}$, $\bar{7}$, $\bar{7}$)] have either removed them well below the continuum limits or have made them marginal candidates to be matched with the measured shells.

(3) The subsidiary minima corrections are shown to give a good explanation of the wave-function density at the donor nucleus, for the first time explaining the donor dependence for As, P, and Sb semiquantitatively. This is accomplished with a simple exponential envelope function rather than employing the sharply peaked Whittaker function and a cutoff radius.

(4) Analysis of the admixture coefficients yields estimates of the energy splittings E_{L_1}-E_{Δ_1} and E_{K_1}-E_{Δ_1} in the range 0.3 to 0.5 eV, about a factor of 2 smaller than predicted by the pseudopotential calculations but in approximate agreement with the $\mathbf{k}\cdot\mathbf{p}$ calculations. Additional refinement of the Fermi contact constant calculations should yield more accurate values of these energy splittings and will also give values of the mass tensors for the subsidiary minima inferred from the anisotropy of the envelope functions for the respective valleys.

(5) The corrections to the energy of the $1s$-A_1 donor state are shown to result primarily from the valley-valley coupling terms and the single-valley correction is shown to be a very small fraction of the total correction. Estimates indicate the subsidiary minima may account for between 25 and 50% of the energy correction to the $1s$-A_1 state.

(6) A component of ψ lacking inversion symmetry has been incorporated into the donor wave function resulting from f function admixed by the tetrahedral potential in the single-valley Schrödinger equation. Although this component is speculative it does lead to some improvement in the over-all fit of the calculated values with the experimental data.

(7) From the ENDOR shell-lattice site matchings evidence is presented which indicates the three-dimensional appearance of the wave-function density reflects to a significant degree the tetrahedral symmetry of the atoms surrounding the donor.

ACKNOWLEDGMENTS

Lively discussions with Dr. E. B. Hale concerning the ENDOR data and their interpretation, from which emerged certain of the ideas presented in this paper, are gratefully acknowledged. The author wishes to thank R. Craven for programming and running the computer calculations of the Fermi contact constants. He is grateful to Dr. F. Ham for a discussion concerning the use of the Whittaker function and for several helpful suggestions concerning the manuscript. Technical assistance from Professor Dr. W. Kanzig and the ETH staff in producing this paper is gratefully ac-

knowledged. Finally, the author greatly appreciates the support of the U. S. Atomic Energy Commission and the John Simon Guggenheim Foundation during the course of this work.

APPENDIX A: COUPLED-VALLEY MATRIX AND SCHRÖDINGER EQUATION

The problem of coupled valleys has been treated previously.[36,33] When considering the coupling between the L_1, K_1, U_1, and Δ_1 minima, one is confronted with a large 30×30 matrix even after reducing the eight L_1 valley ψ_j to four functions, the 12 K_1 valley ψ_j to six functions, and the 24 U_1 "valley" ψ_j to 12 functions (the U_1 valleys may be further reduced if the four regions on a single XUW face are lumped together). Since we consider only first-order perturbation theory and are only concerned with the coupling of the L_1, K_1, and U_1 valleys to the Δ_1 valleys, the coupling between the different subsidiary minima can be neglected. We consider as an example the coupling between the K_1 and Δ_1 valleys. The approach is readily extended to the L_1 and U_1 valleys. The 12×12 valley-valley coupling matrix will have the form

$$H_{VO}=-$$

	x	$-x$	y	$-y$	z	$-z$	$xy,\ \bar{x}\bar{y}$	$x\bar{y},\ \bar{x}y$	$yz,\ \bar{y}\bar{z}$	$y\bar{z},\ \bar{y}z$	$zx,\ \bar{z}\bar{x}$	$z\bar{x},\ \bar{z}x$
	W	Δ_o	Δ_a	Δ_a	Δ_a	Δ_a	σ	σ	σ'	σ'	σ	σ
	Δ_o	W	Δ_a	Δ_a	Δ_a	Δ_a	σ	σ	σ'	σ'	σ	σ
Δ_1	Δ_a	Δ_a	W	Δ_o	Δ_a	Δ_a	σ	σ	σ	σ	σ'	σ'
	Δ_a	Δ_a	Δ_o	W	Δ_a	Δ_a	σ	σ	σ	σ	σ'	σ'
	Δ_a	Δ_a	Δ_a	Δ_a	W	Δ_o	σ'	σ'	σ	σ	σ	σ
	Δ_a	Δ_a	Δ_o	Δ_a	Δ_o	W	σ'	σ'	σ	σ	σ	σ
	σ	σ	σ	σ	σ'	σ'	W'	ρ_s	ρ_a	ρ_a	ρ_a	ρ_a
	σ	σ	σ	σ	σ'	σ'	ρ_s	W'	ρ_a	ρ_a	ρ_a	ρ_a
K_1	σ'	σ'	σ	σ	σ	σ	ρ_a	ρ_a	W'	ρ_s	ρ_a	ρ_a
	σ'	σ'	σ	σ	σ	σ	ρ_a	ρ_a	ρ_s	W'	ρ_a	ρ_a
	σ	σ	σ'	σ'	σ	σ	ρ_a	ρ_a	ρ_a	ρ_a	W'	ρ_s
	σ	σ	σ'	σ'	σ	σ	ρ_a	ρ_a	ρ_a	ρ_a	ρ_s	W'

(A1)

Each 6×6 matrix for the Δ_1 and K_1 valleys separately is diagonalized by the same matrix A_{ij}, namely, that formed from the α_j for the A_1, E, and T_2 states (see Appendix C in HC or Ref. 2). Thus the 12×12 matrix B_{ij} consisting of the two identical blocks A_{ij} will diagonalize matrix (A1) into the six states A_1, E, and T_2 but will leave off-diagonal elements showing the coupling between the Δ_1 and K_1 states. Noting that $B_{ij}=A_{ij}$ for $i=1$–6, $j=1$–6; $i=7$–12, $j=7$–12; and also that $B_{ij}=0$ for $i=1$–6, $j=7$–12; $i=7$–12, $j=1$–6; and employing $\Lambda_{lk}'=B_{li}^{-1}\Lambda_{ij}B_{jk}$, we have as shown on p. 4939.

By reducing the K_1 matrix to a 6×6 matrix (taking symmetric combinations of xy and $\bar{x}\bar{y}$, etc.), we have eliminated certain odd-parity states, which accounts for the absence of coupling between the T_2 states of the Δ_1 and K_1 valleys. Secondly, this reduction also means that the matrix element between x and $(xy+\bar{x}\bar{y})$ actually consists of two matrix elements, namely, $\sigma=\sigma_a+\sigma_o$, and the matrix element between z and $(xy+\bar{x}\bar{y})$ also consists of two identical matrix elements σ_m. Here a means adjacent and is the smallest $|\mathbf{k}_i-\mathbf{k}_j|$ between Δ_1 and K_1 minima, o means opposite and refers to the largest $|\mathbf{k}_i-\mathbf{k}_j|$ between Δ_1 and K_1 minima, m means middle corresponding to an intermediate value of $|\mathbf{k}_i-\mathbf{k}_j|$ between the Δ_1 and K_1 minima. Thus we have

$$\langle A_{1-K_1}|\,U(r)\,|A_{1-\Delta_1}\rangle=-(4\sigma_a+4\sigma_m+4\sigma_o), \quad \text{(A3)}$$

which viewed from the point of view of a single Δ_1 minimum just represents the symmetric sum of the coupling with the 12 different K_1 valleys. Similarly, the coupling between the E states is proportional to $(\sigma_a+\sigma_o-2\sigma_m)$, which is much smaller than Eq. (A3)

$$H_{VO}' = -$$

	Δ_1 A_1	E_a	E_b	T_{2x}	T_{2y}	T_{2z}	K_1 A_1	E_a	E_b	T_{2xy}	T_{2yz}	T_{2zx}
	$W+4\Delta_a+\Delta_o$	0	0	0	0	0	$4\sigma+2\sigma'$	0	0	0	0	0
	0	$W+\Delta_o-2\Delta_a$	0	0	0	0	0	$\sigma-\sigma'$	$\sqrt{3}(\sigma-\sigma')$	0	0	0
	0	0	$W+\Delta_o-2\Delta_a$	0	0	0	0	$\sqrt{3}(\sigma-\sigma')$	$-(\sigma-\sigma')$	0	0	0
Δ_1	0	0	0	$W-\Delta_o$	0	0	0	0	0	0	0	0
	0	0	0	0	$W-\Delta_o$	0	0	0	0	0	0	0
	0	0	0	0	0	$W-\Delta_o$	0	0	0	0	0	0
	$4\sigma+2\sigma'$	0	0	0	0	0	$W'+4\rho_a+\rho_s$	0	0	0	0	0
	0	$\sigma-\sigma'$	$\sqrt{3}(\sigma-\sigma')$	0	0	0	0	$W'+\rho_s-2\rho_a$	0	0	0	0
	0	$\sqrt{3}(\sigma-\sigma')$	$-(\sigma-\sigma')$	0	0	0	0	0	$W'+\rho_s-2\rho_a$	0	0	0
K_1	0	0	0	0	0	0	0	0	0	$W'-\rho_s$	0	0
	0	0	0	0	0	0	0	0	0	0	$W'-\rho_s$	0
	0	0	0	0	0	0	0	0	0	0	0	$W'-\rho_s$

(A2)

since one expects the σ's to all have the same sign and be the same order of magnitude. If the above type of analysis is extended to the L_1 and U_1 valleys one obtains

$$\langle A_{1-L_1} \mid U(\mathbf{r}) \mid A_{1-\Delta_1}\rangle = -(4\lambda_a+4\lambda_o) \quad \text{(A4)}$$

and

$$\langle A_{1-U_1} \mid U(\mathbf{r}) \mid A_{1-\Delta_1}\rangle = -(4\mu_a+8\mu_{m1}+8\mu_{m2}+4\mu_o). \quad \text{(A5)}$$

The a and o have the same meaning; however, for the U_1 valleys there are two slightly different intermediate $|\mathbf{k}_i-\mathbf{k}_j|$ designated $m1$ and $m2$. These $|\mathbf{k}_i-\mathbf{k}_j|$ can best be visualized in Fig. 2. Equations (A4) and (A5), viewed from the standpoint of a single Δ_1 minimum, represent the coupling with the eight different L_1 valleys and the 24 different U_1 valleys.

Starting with $[H_0+U(r)]\psi_b=E\psi_b$, in which ψ_b is the sum $\sum_j\alpha_j\psi_j$ over all valleys, one can derive an approximate coupled-valley Schrödinger equation of the form

$$\alpha_l[E_l(i\nabla)+U(r)-E]F_l(\mathbf{r}) + \sum_{j\neq l}\alpha_j \exp[i(\mathbf{k}_j-\mathbf{k}_l)\cdot\mathbf{r}]U(r)F_j(\mathbf{r})=0. \quad \text{(A6)}$$

This equation is similar to the coupled-valley equation of Twose[70] but differs in two respects: (1) the sum over coupled valleys is now a sum over all coupled valleys including the higher-energy subsidiary valleys; (2) terms of the form

$$\sum_{j\neq l}\alpha_j \exp(-i\mathbf{k}_l\cdot\mathbf{r})(H_0-E)\exp(i\mathbf{k}_j\cdot\mathbf{r})F_j(r)$$

have been neglected compared to the potential-energy term $\exp[i(\mathbf{k}_j-\mathbf{k}_l)\cdot\mathbf{r}]\ U(r)$ in the valley-coupling term. This can be justified by multiplying the valley-coupling term by $F_l(\mathbf{r})^*$ and integrating over the spatial coordinates. The result for the neglected term is $\sum_{j\neq l}\alpha_j(E_j(i\nabla)-E)S_{jl}$, where S_{jl} is the valley overlap integral between the jth and lth valleys. The potential-energy term takes the form $\sum_{j\neq l}\alpha_j V_{jl}$, where

$$V_{jl}=\int F_l(\mathbf{r})^* \exp(-i\mathbf{k}_l\cdot\mathbf{r})U(r)\exp(i\mathbf{k}_j\cdot\mathbf{r})F_j(\mathbf{r})d\tau,$$

(see Sec. IV D) and is of order several meV. The overlap integrals are very small (see Appendix B) justifying the neglect of these terms. This result emphasizes that it is $U(r)$ which couples the different valleys. The α_l and α_j are determined by T_d symmetry and also by the valley coupling.

Equation (A6) contains the effective valley-coupling potential $\exp[i(\mathbf{k}_j-\mathbf{k}_l)\cdot\mathbf{r}]\ U(r)$ while the valley-valley coupling matrix (A1) contains the matrix elements V_{jl}. The diagonalization of an expanded (A1) will determine the energy of the different coupled-valley states; however, to find $F_l(\mathbf{r})$ we must solve the set of coupled equations (A6) with l summed over all the valleys being considered. This problem can only be treated approximately.

First, it is convenient to average the coupling potential over solid angles to remove the angular dependence. This yields

$$\langle \exp[i(\mathbf{k}_j-\mathbf{k}_l)\cdot r]U(r)\rangle_\Omega = U(r)\sin(|\mathbf{k}_j-\mathbf{k}_l|r)/|\mathbf{k}_j-\mathbf{k}_l|r.$$

One has a large effective potential for $|\mathbf{k}_j-\mathbf{k}_l|r<\pi/2$, while for $r>a$ ($a=5.43$ Å), the potential is much weaker than $U(r)$. To understand the effect of the valley-valley coupling on $F_l(\mathbf{r})$ it is sufficient for our purposes to treat only the six Δ_1 minima. Then the equation for $F_z(r)$ will have the form

$$\left[\frac{\hbar^2}{2m_t}\frac{\partial^2}{\partial z^2}-\frac{\hbar^2}{2m_t}\left(\frac{\partial^2}{\partial x^2}+\frac{\partial^2}{\partial y^2}\right)+U(r)-E\right]F_z(\mathbf{r}) = -\left[U(r)\frac{\sin(\Delta k_o r)}{\Delta k_o r}F_{-z}(\mathbf{r})+U(r)\frac{\sin(\Delta k_a r)}{\Delta k_a r} \times(F_x(\mathbf{r})+F_{-x}(\mathbf{r})+F_y(\mathbf{r})+F_{-y}(\mathbf{r}))\right]. \quad \text{(A7)}$$

The equations for the other five Δ_1 minima will have the same form. Taking the totally symmetric summation of the six coupled equations yields

$$\left\{-\frac{h^2}{2m^*}\nabla^2+U(r) \times\left[1+4\frac{\sin(\Delta k_a r)}{\Delta k_a r}+\frac{\sin(\Delta k_o r)}{\Delta k_o r}\right]-E\right\}G(\mathbf{r}) \times\sum_{x_i=x,y,z\ \text{cyclic}}-\tfrac{1}{2}\hbar^2\left[\left(\frac{1}{m_t}-\frac{1}{m^*}\right)\frac{\partial^2}{\partial x_i^2}+\left(\frac{1}{m_t}-\frac{1}{m^*}\right) \times\left(\frac{\partial^2}{\partial x_j^2}+\frac{\partial^2}{\partial x_k^2}\right)\right](F_{x_i}+F_{-x_i})=0, \quad \text{(A8)}$$

where

$$G(\mathbf{r})=F_x(\mathbf{r})+F_{-x}(\mathbf{r})+F_y(\mathbf{r}) +F_{-y}(\mathbf{r})+F_z(\mathbf{r})+F_{-z}(\mathbf{r}).$$

The last terms in the sum are anisotropic kinetic-energy terms and are expected to be small since m^* is intermediate between m_t and m_t. $G(\mathbf{r})$ transforms as the A_1 representation of T_d symmetry and has a large spherical component, namely, the isotropic component of $F_j(\mathbf{r})$ for the Δ_1 minima. Neglecting the anisotropic kinetic-energy terms, $G(\mathbf{r})$ is the solution of a Schrödinger equation with an eigenvalue $E_{1s-A_1}'=-E_0-(4\Delta_a+\Delta_o)$, not the same as E_{1s-A_1} in Eq. (33) because of the neglect of the subsidiary minima and the small self-valley correction. Neglecting the valley coupling potential, and setting $U(r)=-e^2/\epsilon_0 r$, the solution is $G(r)=(1/\pi a^{*3})^{1/2}\exp(-r/a^*)$ with eigenvalue $-E_0$. An average solution to (A8) will be

$$G'(r)=(1/\pi n'^3 a^{*3})^{1/2}\exp(-r/n'a^*)$$

with eigenvalue $E_{1s-A_1}'=-E_0(1/n'^2)$ if the average

effect of the total potential results in a stronger potential $-e^2/\epsilon_0 r(1/n')$. Quantitatively, it is difficult to describe accurately the effect on $F_j(\mathbf{r})$ of the extra potential $\delta U(\mathbf{r})$ and the oscillatory coupling potential. Qualitatively, one might expect $G(r)$ to be nonexponential for small r and also to have small oscillatory components. The consideration of the subsidiary valleys will further enhance the potential and will lead to the b^* function for $F_j(r)$ with $n=(E_0/E_{1s-A_1\text{-expt}})^{1/2}$.

APPENDIX B: OVERLAP INTEGRALS BETWEEN VALLEYS

The overlap integral between the jth and lth valleys has the form

$$S_{jl}=\int F_l(\mathbf{r})^* u_{\mathbf{k}_l}(r)\exp(-i\mathbf{k}_l\cdot r)\times F_j(\mathbf{r})u_{\mathbf{k}_j}(r)\exp(i\mathbf{k}_j\cdot\mathbf{r})d\tau$$
$$\approx\int F_l(\mathbf{r})^* F_j(\mathbf{r})\exp[i(\mathbf{k}_j-\mathbf{k}_l)\cdot\mathbf{r}]d\tau, \quad \text{(B1)}$$

where in the second form the periodic Bloch function has been removed. Although the integrals are very difficult for anisotropic envelope functions they are straightforward for spherical isotropic envelope functions and we use the b^* form $(1/\pi b^{*3})^{1/2}\exp(-r/b^*)$ here. Then S_{jl} has the form

$$S_{jl}\approx[\tfrac{1}{4}(|\mathbf{k}_l-\mathbf{k}_j|^2 b^{*2})+1]^{-2}. \quad \text{(B2)}$$

One might argue that we should set $n=1$ and $b^*=na^*=a^*$, that is, use the uncorrected $F_j(r)$ to compute these matrix elements; however, we compute them for $n=0.80$ (case of P) for the closest valleys (adjacent valleys designated by a) in $\mathbf{k}$ space in the BZ. We find $S_{\Delta_1-\Delta_1)_a}=6.7\times10^{-5}$, $S_{\Delta_1-L_1)_a}=3.8\times10^{-4}$, $S_{\Delta_1-K_1)_a}=4.6\times10^{-4}$, and $S_{\Delta_1-U_1)_a}=7.6\times10^{-3}$. Thus all the overlap integrals except $S_{\Delta_1-U_1)_a}$ are less than 10^{-3} and it is less than 10^{-2}. This indicates the neglect of overlap terms, even considering anisotropic envelope functions, seems to be an excellent approximation, even though we are considering valleys closer in $\mathbf{k}$ space than the six Δ_1 valleys.

* Supported in part by the U.S. Atomic Energy Commission.
† Work completed at the Laboratorium für Festkörperphysik, Eidg. Technische Hochschule, Zurich, Switzerland, while the author was a John Simon Guggenheim Foundation Fellow.

[1] W. Kohn and J. M. Luttinger, Phys. Rev. **98,** 915 (1955); for a discussion of effective mass theory, see J. M. Luttinger and W. Kohn, *ibid.* **97,** 969 (1955).
[2] See W. Kohn, in *Solid State Physics*, edited by F. Seitz and D. Turnbull (Academic, New York, 1957); for an accurate determination of the ground state $1s$-A_1 energy levels, see R. L. Aggarwal and A. K. Ramdas, Phys. Rev. **140,** A1246 (1965).
[3] The potential deviates from Coulombic form and must approach $-(Z_{\text{donor}}-Z_{\text{Si}})e^2/r$ as $r\to0$. The potential is only considered to deviate strongly inside a central cell with a radius of order of the Wigner-Seitz cell.
[4] W. Kohn and J. M. Luttinger, Phys. Rev. **97,** 883 (1955).
[5] G. Weinreich, J. Phys. Chem. Solids **8,** 216 (1959).
[6] P. Csavinsky, J. Phys. Chem. Solids **24,** 1003 (1963).
[7] J. Appel, Phys. Rev. **133,** A280 (1964).
[8] K. Muller, Solid State Commun. **2,** 205 (1964).
[9] A. Morita and H. Nara, J. Phys. Soc. Japan Suppl. **21,** 234 (1966).
[10] R. C. Fletcher, W. A. Yager, G. L. Pearson, A. W. Holden, W. T. Read, and F. R. Merritt, Phys. Rev. **94,** 1392 (1954); R. C. Fletcher, W. A. Yager, G. L. Pearson, and F. R. Merritt, *ibid.* **95,** 844 (1954); G. Feher, *ibid.* **114,** 1219 (1959).
[11] E. B. Hale and R. L. Mieher, Phys. Rev. **184,** 739 (1969).
[12] G. Feher, Phys. Rev. **114,** 1219 (1959).
[13] Attributed by Feher (Ref. 12) to Schechter and Mozer (unpublished).
[14] E. B. Hale and R. L. Mieher, Phys. Rev. **184,** 751 (1969).
[15] Shell K was matched as (0, 0, 8) on the basis of symmetry and resonable agreement for the Fermi contact constant; however, there are very few ⟨001⟩-axis sites to consider.
[16] E. B. Hale and T. G. Castner, Jr., Phys. Rev. B **1,** 4763 (1970).
[17] The uniaxial stress effect on ENDOR shells A, B, and K, already previously matched (Refs. 12 and 11) by symmetry and the Fermi contact constants, were in good agreement with theory based on just the six Δ_1 minima and yielded $k_0/k_{\max}=0.86\pm0.02$.
[18] E. B. Hale and R. L. Mieher, Phys. Letters **29A,** 350 (1969); Phys. Rev. B (to be published).
[19] In the lowest conduction band L_1 is a true minimum; the K_1 and $U_1(K_1')$ points need not from symmetry considerations be true minima and saddle points, respectively, because the band energy may vary linearly away from these points in certain directions.
[20] R. F. Bacher, Phys. Rev. **43,** 264 (1933); see also C. W. Ufford, *ibid.* **44,** 732 (1933); A. G. Shenstone and H. N. Russel, *ibid.* **39,** 415 (1932).
[21] G. F. Koster and J. C. Slater, Phys. Rev. **95,** 1167 (1954).
[22] H. Kaplan, J. Phys. Chem. Solids **24,** 1593 (1963).
[23] G. A. Peterson, in *Proceedings of the Seventh International Conference on the Physics of Semiconductors, Paris, 1964* (Dunod, Paris, 1964), p. 771.
[24] F. Bassani, G. Iadonisi, and B. Preziosi, Phys. Rev. **186,** 735 (1969).
[25] G. W. Ludwig, Phys. Rev. **137,** 1520 (1965).
[26] H. Nara, J. Phys. Soc. Japan **20,** 778 (1965).
[27] L. Kleinman and J. C. Phillips, Phys. Rev. **118,** 1153 (1960).
[28] D. Brust, Phys. Rev. **134,** A1337 (1964).
[29] Marvin L. Cohen and T. K. Bergstresser, Phys. Rev. **141,** 789 (1966).
[30] E. O. Kane, Phys. Rev. **146,** 558 (1966).
[31] Manuel Cardona and Fred H. Pollak, Phys. Rev. **142,** 530 (1966).
[32] G. Dresselhaus and M. S. Dresselhaus, Phys. Rev. **160,** 649 (1967).
[33] D. K. Wilson and G. Feher, Phys. Rev. **124,** 1068 (1961).
[34] See Ref. 2.
[35] δU must transform according to T_d symmetry and will be composed of spherical, tetrahedral, and cubic components, the spherical component being much the strongest in the central cell.
[36] The valley-valley interaction for the six Δ_1 minima was first considered by P. J. Price, Phys. Rev. **104,** 1223 (1956). In addition to this correction there is a single-valley correction resulting from δU, and finally the correction resulting from the admixture of subsidiary minima.
[37] L_1 will be characterizcd by an energy ellipsoid with two masses m_l and m_t. Estimates of these masses have been made in Refs. 31 and 32.
[38] While the band calculations indicate a valley with K_1 an energy minimum, the energy can vary linearly with $\mathbf{k}$ away from K_1 along Σ and also away from K_1 along KL (see Ref. 32). If the linear terms are small one can still use the Schrödinger equation in Eq. (4) and treat the linear terms by perturbation theory. The magnitude of these linear terms is not well known and seems to vary substantially in the different band calculations.
[39] We employ the usual notation; see L. P. Bouckaert, R. Smoluchowski, and E. Wigner, Phys. Rev. **50,** 58 (1936). This point is sometimes denoted K' (see Ref. 30), which is, perhaps, more logical because of the 2-to-1 correspondence with the K points.
[40] Strictly speaking U_1 need not be a saddle point because the energy can vary linearly away from U_1 along Σ' and also in the direction toward L_1. Nevertheless, there is a large density of states of relatively low energy in the vicinity of the numerous U_1 points.
[41] The degeneracy of the Δ_2' and Δ_1 band energy curves at X_1 might be considered a serious problem, particularly because at k_0 $\Delta_{2'}$ is only about 0.4 eV above the Δ_1 minima. This is not

thought to be a problem, because if an extended zone scheme were employed $\Delta_{2'}$ would be the extension of Δ_1 beyond X_1, and therefore could be considered the higher-energy portion associated with the Δ_1 minima.

[42] M. Morse, *Functional Topology and Abstract Variational Theory, Memorial Sciences Mathématique* (Gauthier-Villars, Paris, 1938), Fasc. 92.

[43] James C. Phillips, Phys. Rev. **104,** 1263 (1956).

[44] The treatment of K_1 and U_1 as minima is not rigorous but allows one to simply calculate approximate corrections for wave function admixture from these two regions of the BZ. Treating U_1 as a minimum actually underestimates the correction from this region along the line U_1X_1 since the true band energy apparently decreases from U_1 toward X_1.

[45] A detailed consideration of the matrix elements shows they can have complex phase factors depending on the particular k_m, but in the product $\langle\psi_m | U(r)|\psi_{KL-1s-A1}\rangle\psi_m$ the phase is determined solely by the phase of $u_{kj}(r)$ for the Δ_1 minima. For the Δ_1 minima the s part of $u_{kj}(\mathbf{r})$ can be chosen real, making it possible to arbitrarily designate the s part of $u_{km}(\mathbf{r})$ real even though the phase of $u_{km}(\mathbf{r})$ and its s part are in general complex. The spherical part of $U(r)$ can only lead to $|A_1\rangle_M$ functions as given in Eqs. (14a)–(14c), which contain linear combinations of cosines resulting from the symmetric sum of Bloch phase factors. No sine terms apparently result from these admixtures and $|A_1\rangle_t$ still has inversion symmetry with respect to the even-integer lattice sites.

[46] E. Fermi, Z. Physik **60,** 320 (1930).

[47] A value of η has been determined experimentally; see R. G. Shulman and B. J. Wyluda, Phys. Rev. **103,** 1127 (1956); see also D. K. Wilson, *ibid.* **134,** A265 (1964), for a small correction to this value.

[48] Hale and Mieher (Ref. 18) noted the "distant" contribution to the dipole-dipole constants resulting from the slow variation of the envelope function was only about 5–10% of the total. This contribution should be even smaller if the b^* envelope functions are employed instead of the more rapidly varying Whittaker functions.

[49] Only this type of d function will yield a nonzero value of B_{xy} for sites (0, 0, 4) and (0, 0, 8) as required by the experimental results (see Refs. 11 and 12). The axial d function $d_{xx} \propto (r^2-3x^2)$ is also allowed along Δ_1 but will qualitatively contribute nothing new.

[50] Assuming $J_2 \approx J_1$, the second term in Eq. (23a) makes much the smaller contribution to B_{zz} for most lattice sites. An important exception occurs for site (2, 2, 0), for which the second term is of opposite sign and much larger than the first term. This second term is essential for the indentification of site (2, 2, 0) with Endor shell $F[V(\mathrm{Sb})]$. Shell F has the largest B_{zz} value of all the measured shells and can be identified by its B_{zz} value if the second term in Eq. (23a) is important. As shown in this paper this identification is also consistent with the Fermi contact constants for site (2, 2, 0). A third term of the same form as the second term, but with the cosines replaced by sines, has also been obtained. This term results only from the pure d_{yz} function, etc., in $u_k(r)$ and is thought to be small.

[51] Using the values of E_{1s-A1} obtained in Ref. 2 and $E_0 = -29$ meV one finds $n(\mathrm{As}) = 0.736$, $n(\mathrm{P}) = 0.800$, and $n(\mathrm{Sb}) = 0.826$. These values were used for the calculations reported in this paper. If the effective mass value E_0 is nearer -32 meV then the n values should be increased somewhat and the envelope functions will be less sharply peaked than those employed here.

[52] $u_k(\mathbf{r})$ in the central cell should be orthogonalized to the core donor states and will have the form $u_k(\mathbf{r}) = u_k^0(\mathbf{r}) - \Sigma_c a_c \phi_c(\mathbf{r})$, where $a_c = \langle u_k^0(\mathbf{r})|\phi_c(\mathbf{r})\rangle$. The net result for As and Sb is that $u_k(\mathbf{r})$ in the central cell becomes similar to the respective atomic wave functions of the donor atom for the outer electron.

[53] The integers 14 and 16 also have large cosine values. However, sites with those integers are very far from the donor. The site (14, 14, 0) has substantial negative corrections from the subsidiary minima. The site (0, 0, 16) has very favorable positive corrections from all three subsidiary minima but the pancake effects reduces these considerably. In any case only two ⟨001⟩-axis-class shells have been measured.

[54] G. D. Watkins and Frank S. Ham, Phys. Rev. B **1,** 4071 (1970).

[55] F. J. Morin, T. H. Geballe, and C. Herring, Phys. Rev. **101,** 525 (1957).

[56] J. E. Aubrey, W. Gubler, J. Henningsen, and S. H. Koenig, Phys. Rev. **130,** 1667 (1963).

[57] I. Balslev, Phys. Rev. **143,** 636 (1966).

[58] R. A. Stradling and V. V. Zhukov, Proc. Phys. Soc. (London) **87,** 263 (1966).

[59] H. Kawamura, S. Fukai, and R. Ito, Phys. Letters **13,** 26 (1964).

[60] By lumping the 4 U_1 valleys on a single XUW face of the BZ together the average effect should be the same as for a Δ_1 valley or the X_1 point. For this reason the wave function for the U_1 "minima" will behave under uniaxial stress in a manner similar to the Δ_1 minima.

[61] This effect was not studied in Ref. 16.

[62] Theodore G. Castner, Phys. Rev. **155,** 816 (1967).

[63] D. Olson, Bull. Am. Phys. Soc. **11,** 186 (1966); D. Olson and T. G. Castner, Jr. (unpublished).

[64] D. W. Olson, Ph.D. thesis, University of Rochester, 1969 (unpublished).

[65] J. C. Hensel, H. Hasegawa, and M. Nakayama, Phys. Rev. **138,** A225 (1965).

[66] W. C. Dunlap, Jr., and R. L. Watters, Phys. Rev. **92,** 1396 (1953); a new value, $\epsilon_0 = 11.4$, has been found by R. A. Faulkner, *ibid.* **184,** 713 (1969), from a careful fitting of the calculated donor excited states with optical data. His analysis yields $E_0 = 31.27$ meV.

[67] This notation is different than that in Ref. 33, where Δ was used for the coupling between adjacent Δ_1 minima and $\Delta(1-\delta)$ for the coupling between opposite Δ_1 minima. Note that the energy splitting between the $1s$-E and $1s$-A_1 states is not $6\Delta_a$ (6Δ in the notation of Ref. 33) because of the second-order contribution from the subsidiary minima. Furthermore, the second-order terms shift the center of gravity of the six $1s$ levels and therefore one cannot determine the single-valley energy correction from the center of gravity of the $1s$ levels.

[68] This relationship is formulated in analogy with that for the isotropic mass and the mass tensor components. One cannot show that this leads to a normalized $(F_z)_{\mathrm{anis}}$ $[\int (F_z)_{\mathrm{anis}}\, d\Omega = 4\pi]$; however, a numerical check for the anisotropies considered here indicates it is an excellent approximation. In Refs. 12 and 14, $(F_z)_{\mathrm{anis}}$ is multiplied by a factor $(a^*/a_l a_{t1} a_{t2})^{1/2}$, where $a^* \neq (a_l a_{t1} a_{t2})^{1/3}$. This procedure raises the question of how these quantities are determined.

[69] M. Lampert, Phys. Rev. **97,** 352 (1955).

[70] See Appendix by W. D. Twose, in H. Fritzsche, Phys. Rev. **125,** 1560 (1962).

[71] $f(r)$ can have the form $1/(b^2+r^2)^n$. Dielectric constant considerations suggest $n > \frac{7}{2}$, making this a very-short-range potential since b is of order of the nearest-neighbor distance.

[72] L. I. Schiff, *Quantum Mechanics* (McGraw-Hill, New York, 1949), p. 85.

[73] Only the cross term contributes to the lack-of-inversion-symmetry effect. The quadratic term from ψ_t is proportional to $(x_l y_l z_l)^2$ and is negligible for most shells but makes small contributions to distant sites like (9, 9, 9).

[74] H. Nara and A. Morita, J. Phys. Soc. Japan **21,** 1852 (1966); see also A. Morita, M. Azuma, and H. Nara, *ibid.* **17,** 1570 (1962).

[75] The screening constants used in Ref. 74 are somewhat different than those used in this work. They seem too small for Sb and As and lead to very different values of a_v in Eq. (44).

[76] F. Herman and S. Skillman, *Atomic Structure Calculations* (Prentice-Hall, Englewood Cliffs, N.J., 1963).

[77] The screening constants used in Ref. 74 lead to even larger values of V_{jl} for both Sb and As, presumably because of inadequate screening in the core region. The effect of lattice distortion on $U(r)$ has not been explicitly considered; however, there is no evidence yet for this effect in the ENDOR data.

[78] V. G. Grachev, M. F. Deigen, and S. I. Pekar, Fiz. Tverd. Tela **9,** 3157 (1967) [Soviet Phys. Solid State **9,** 2489 (1968)].

[79] See the review article by H. Seidel and H. C. Wolf, in *Physics of Color Centers*, edited by W. Beall Fowler (Academic, New York 1968).